RESTRAINING POST-LIQUEFACTION FLOW DEFORMATIONS

PHASE II

by

W.D. Liam Finn

June 15, 1994

United States Army

EUROPEAN RESEARCH OFFICE OF THE U.S. ARMY

London, England

Contract No.: *DAJA45-93-C-0038*

CORK GEOTECHNICS LTD.

RESTRAINING POST-LIQUEFACTION FLOW DEFORMATIONS

PHASE II

by

W.D. Liam Finn

June 15, 1994

United States Army

EUROPEAN RESEARCH OFFICE OF THE U.S. ARMY

London, England

Contract No.: *DAJA45-93-C-0038*

CORK GEOTECHNICS LTD.

CHAPTER 1

INTRODUCTION

Review of Phase I Studies

This report describes studies conducted for Phase II of the project "Restraining Post-Liquefaction Flow Deformations". To provide a context for this report, the background of the project will be reviewed briefly and some key findings from the first phase will be presented.

In Phase I of the project, studies were focussed on the use of piles to restrain flow deformations. This topic was of considerable interest to the US Army Corps of Engineers because pile-nailing of the upstream slope of Sardis Dam in Mississippi was being considered as an option for restraining sliding of the slope on a potentially liquefiable thin layer in the foundation (Finn et al., 1991).

The key factors controlling the feasibility and cost of pile installations to restrain flow deformations are pile length and spacing, stiffness and strength of unliquefied soils surrounding the piles, residual strength of liquefied soils, the geometry of the structure, and the intensity of shaking after liquefaction has occurred. The ability to analyze such a complex problem while taking into account nonlinear behaviour of soil, potentially large strain deformations in unremediated parts of the structure and a realistic interaction between piles and soil during both static and seismic loading is the essential requirement for determining the best location for the piles, an appropriate length and size and for categorizing the effects of soil properties.

Very little is known about the behaviour of piles under these complex conditions. Most of the evidence is from Japan where pile foundations have been severely damaged in liquefied ground as a result of ground displacements. However these piles were designed for vertical static loading

only and both piles and the connections to the pile caps were inadequately designed to resist horizontal loading. Piles in Oakland Harbor were similarly damaged during the Loma Prieta Earthquake of 1989. Therefore there is a need for detailed analytical studies of pile installations to provide much needed information on the potential performance of piles under these demanding situations and hence provide a framework of understanding for design of cost effective remediation measures.

The computer programs TARA-3 (Finn et al., 1986) and TARA-3FL (Finn and Yogendrakumar, 1989) were used to conduct the studies in Phase I. It was the first time such analyses had been performed. The findings of the Phase I studies were used to develop the design requirements for the piles for remediating Sardis Dam. The pile design resulted in very substantial savings in remediation costs compared to alternative proposals. The design would not have been feasible without the Phase I studies.

The studies for Sardis Dam could be conducted using the plane strain 2-D analyses in the TARA-3 suite of programs because remediation was necessary across a long longitudinal section of the dam. Where such conditions do not hold, 3-D analyses are necessary.

Full 3-D nonlinear dynamic analysis of pile groups is not a feasible proposition for engineering practice at present. It makes impractical demands on computational speed and capacity and renders the extension to dynamic effective stress analysis extremely difficult. Full 3-D analysis also inhibits the detailed parametric studies which are so important in exploring cost-efficient remediation options. A simplified model for the 3-D soil continuum under horizontal shaking by vertically propagating shear waves has been developed which overcomes these difficulties. This simplified 3-D model captures the significant motions and stresses in foundation

soils with acceptable accuracy during ground shaking and provides the basis for significant advances in the seismic analysis of piles.

This report is restricted to describing the evolution and validation of a proposed simplified 3-D method of analysis of the dynamic response of piles that greatly reduces the computational demands for solving practical problems. It is not a state-of-the-art study of the dynamic response of pile foundations. References to the literature are restricted primarily to case studies used for validation.

Structure of Report

A general simplified model of the dynamic response of the soil continuum is presented first. Then particular models based on different simplifying assumptions (Matsuo and Ohara, 1960; Veletsos and Younan, 1994; Finn and Wu, 1994; Finn et al., 1994a,b) are derived from the general case. The performance of these models is assessed using the classic solution of Wood (1973) for the dynamic pressures against rigid walls by a homogeneous elastic backfill. The validation study indicates that the proposed simplified model performs very well over a wide range of soil properties. The solution for rigid walls has important applications in remediation studies in its own right. A generally useful remediation measure is the inclusion of concrete plugs such as slurry walls to restrain soil deformations. Assessment of the stability of such walls requires estimates of the seismic lateral pressures. This type of remediation was one of the options considered for Sardis Dam.

The model is modified to accommodate piles in the continuum. The equations of motion for the soil-pile system are formulated in terms of finite elements. Elastic solutions for pile impedances are validated against the full 3-D solutions by Kaynia and Kausel (1982).

The model is extended to nonlinear response by ensuring compatibility between soil strains and the strain dependent moduli and damping of soils continuously during dynamic analysis. This is a major modification of the equivalent linear method used in computer programs such as SHAKE (Schnabel et al., 1972).

The proposed method of analysis is also validated using data from a forced vibration test on a Franki pile conducted at the Pile Research Facility of the University of British Columbia (Sy and Siu, 1992). Data from centrifuge tests on pile foundations under strong shaking conducted at the California Institute of Technology (Gohl, 1991; Finn and Gohl, 1987) allow validation of the proposed method of analysis when nonlinear soil effects are important. For the first time, the variation of pile stiffness and damping with time are traced during strong shaking.

Finally, extensions of the method will be discussed. These extensions include analysis of pile groups, rocking effects and dynamic effective stress analysis.

CHAPTER 2

SIMPLIFIED EQUATIONS FOR DYNAMIC RESPONSE OF FOUNDATION SOILS

The soil is assumed to be a homogeneous, isotropic, elastic solid with a shear modulus G and a Poisson's ratio ν. The equation of motion for the soil continuum in the horizontal direction, x, is written as

$$\frac{\partial \sigma_x}{\partial x} + \frac{\partial \tau_{yx}}{\partial y} = \rho \frac{\partial^2 u}{\partial t^2} \tag{2.1}$$

where σ_x is the normal stress in the x direction and τ_{xy} is the shear stress in the x-y plane.

For two-dimensional plane strain conditions, the stress components are related to the displacements by

$$\sigma_x = \frac{2G}{1-2\nu}\left[(1-\nu)\frac{\partial u}{\partial x} + \nu \frac{\partial v}{\partial y}\right] \tag{2.2}$$

$$\sigma_y = \frac{2G}{1-2\nu}\left[(1-\nu)\frac{\partial v}{\partial y} + \nu \frac{\partial u}{\partial x}\right] \tag{2.3}$$

$$\tau_{xy} = G\left(\frac{\partial u}{\partial y} + \frac{\partial v}{\partial x}\right) \tag{2.4}$$

Then the governing equation, Eq. 2.1, for undamped free vibration of the backfill may be written as

$$\theta G\frac{\partial^2 u}{\partial x^2}+G\frac{\partial^2 u}{\partial y^2}=\rho\frac{\partial^2 u}{\partial t^2} \tag{2.5}$$

where ρ is the mass density of the backfill soil, t is time and θ is a function of Poisson's ratio ν.

The expression for θ depends on the approximations used in modelling the dynamic response of the soil continuum. Three different approximations will be considered.

i) $\nu = 0$

It is assumed that there is no (vertical) displacement in the y-direction. Applying this assumption to Eq. 2.2 and Eq. 2.4 gives

$$\sigma_x=\frac{2(1-\nu)}{1-2\nu}G\frac{\partial u}{\partial x} \tag{2.6}$$

$$\tau_{xy}=G\frac{\partial u}{\partial y} \tag{2.7}$$

Substituting Eq. 2.6 and Eq. 2.7 into Eq. 2.1 and comparing with Eq. 2.5, one finds

$$\theta=\frac{2(1-\nu)}{1-2\nu} \tag{2.8}$$

ii) $\sigma_y = 0$

Here it is assumed that the dynamic normal stresses, σ_y, in the vertical direction are negligible. Applying the assumption to Eq. 2.3, one finds that

$$\frac{\partial v}{\partial y} = -\frac{\nu}{1-\nu}\frac{\partial u}{\partial x} \tag{2.9}$$

Then from Eq. 2.2 and Eq. 2.4 one obtains.

$$\sigma_x = \frac{2}{1-\nu} G \frac{\partial u}{\partial x} \tag{2.10}$$

$$\frac{\partial \tau_{xy}}{\partial y} = G\frac{\partial^2 u}{\partial y^2} - G\frac{\nu}{1-\nu}\frac{\partial^2 u}{\partial y^2} \tag{2.11}$$

Substituting Eq. 2.10 and Eq. 2.11 into Eq. 2.1 and comparing with Eq. 2.5, one finds

$$\theta = \frac{2-\nu}{1-2\nu} \tag{2.12}$$

iii) Proposed Method (Wu, 1993)

In this method the condition $\sigma_y = 0$ is combined with the assumption that the layered half-space behaves as a shear beam. The latter assumption implies that

$$\tau_{xy} = G\frac{\partial u}{\partial y} \tag{2.13}$$

The normal stress σ_x is found by assuming $\sigma_y = 0$ in Eq. 2.3.

$$\sigma_x = \frac{2}{1-\nu} G\frac{\partial u}{\partial x} \tag{2.14}$$

Substituting Eq. 2.13 and Eq. 2.14 into Eq. 2.1 and comparing with Eq. 2.5, one finds

$$\theta = \frac{2}{1-\nu} \tag{2.15}$$

These three different approximations to the response of the layered half-space are incorporated in the general expression for the equations of motion (Eq. 2.5) by the parameter θ.

The capability of different approximations to the response of the soil continuum will now be verified using solutions to the classic problem of dynamic pressures against a rigid wall.

CHAPTER 3

DYNAMIC ANALYSIS OF RIGID WALL-SOIL SYSTEM

Figure 3.1(a) shows the geometry of the problem and its boundary conditions. A uniform elastic soil layer is confined by two vertical rigid walls at its two side boundaries and a rigid base. The soil layer has a total length of 2L and height of H. The original wall-soil problem can be represented by half the structure because of the antisymmetric conditions. The equivalent problem is shown in Fig. 3.1(b), and this is the physical model that will be analyzed. The ground acceleration, $\ddot{u}_0(t)$ is input at the base of the wall-soil system.

Assume the displacement solution of Eq. 2.5 has the form

$$u(x,y,t) = \sum\sum (A \cdot \sin a_m x + B \cdot \cos a_m x)(C \cdot \sin b_n y + D \cos b_n y) \cdot Y_{mn}(t) \qquad (3.1)$$

Applying the boundary conditions

$$u = 0 \text{ ..... at } y = 0 \qquad (3.2a)$$

$$u = 0 \text{ ..... at } x = 0 \qquad (3.2b)$$

The constants B and D are determined to be zero, so

$$u(x,y,t) = \sum\sum C_1 \cdot \sin a_m x \cdot \sin b_n y \cdot Y_{mn}(t) \qquad (3.3)$$

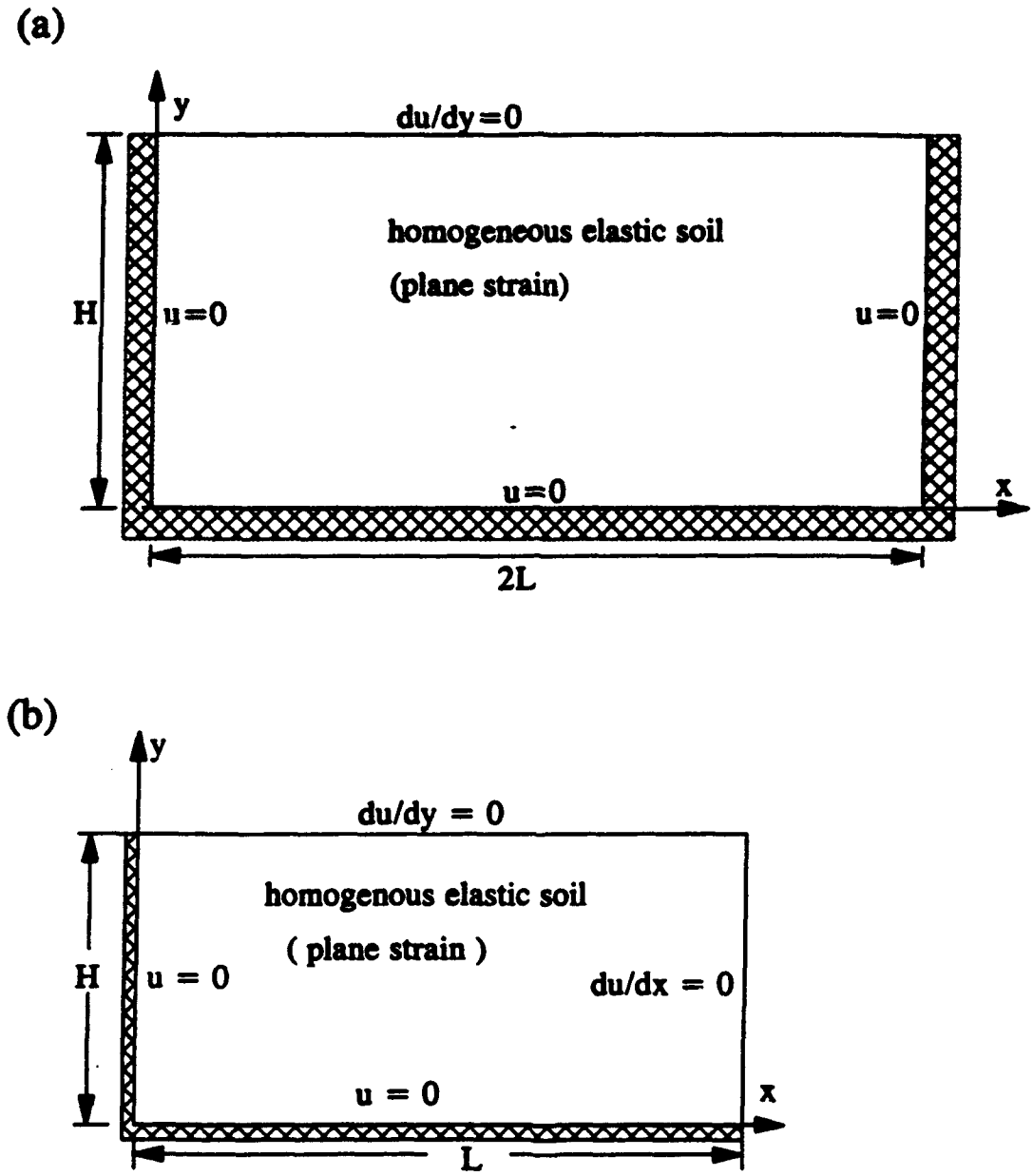

Fig. 3.1. Definition of rigid-wall system: (a) original system; (b) equivalent system using antisymmetric condition.

$$\frac{\partial u}{\partial x} = \sum\sum C_1 a_m \cdot \cos a_m x \cdot \sin b_n y \cdot Y_{mn}(t) \qquad (3.4)$$

$$\frac{\partial u}{\partial y} = \sum\sum C_1 b_n \cdot \sin a_m x \cdot \cos b_n y \cdot Y_{mn}(t) \qquad (3.5)$$

Applying the other two boundary conditions

$$\frac{\partial u}{\partial x} = 0 \ldots\ldots \text{at } x = L \qquad (3.6a)$$

and

$$\frac{\partial u}{\partial y} = 0 \ldots\ldots \text{at } y = H \qquad (3.6b)$$

one obtains

$$a_m \cdot \cos a_m L = 0 \qquad (3.7a)$$

and

$$b_n \cdot \cos b_n H = 0 \qquad (3.7b)$$

therefore,

$$a_m = \frac{(2m-1)\pi}{2L} \qquad (3.8a)$$

and

$$b_n = \frac{(2n-1)\pi}{2H} \qquad (3.8b)$$

The mode shape functions are written as

$$\Phi_{mn}(x,y) = C_1 \cdot \sin a_m x \sin b_n y \tag{3.9}$$

and the displacement solution becomes

$$u(x,y,t) = \sum\sum \Phi_{mn}(x,y) \cdot Y_{mn}(t) \tag{3.10}$$

Substituting Eq. 3.10 into Eq. 2.5, one obtains

$$-G(\theta a_m^2 + b_n^2) \cdot Y_{mn}(t) = \rho \ddot{Y}_{mn}(t) \tag{3.11a}$$

$$-\frac{G}{\rho}(\theta a_m^2 + b_n^2) = \frac{\ddot{Y}_{mn}(t)}{Y_{mn}(t)} = -\omega_{mn}^2 \tag{3.11b}$$

The natural frequencies of the system are found to be

$$\omega_{mn}^2 = \frac{G}{\rho}(\theta a_m^2 + b_n^2) \tag{3.12}$$

The frequency of the first mode is

$$\omega_{11}^2 = \frac{G\pi^2}{4\rho H^2}(1+\theta\frac{H^2}{L^2}) \tag{3.13}$$

In the case of undamped forced vibration caused by a ground acceleration $\ddot{u}_0(t)$, the governing equation becomes

$$\rho\frac{\partial^2 u}{\partial t^2} - (\theta G\frac{\partial^2 u}{\partial x^2} + G\frac{\partial^2 u}{\partial y^2}) = -\rho\ddot{u}_0(t) \tag{3.14}$$

Substituting Eq. (3.10) into Eq. (3.14), multiplying the equation by the mode shape functions, and integrating over the domain, one obtains

$$\begin{aligned}\iint \rho\sum\sum \Phi_{ij}\ddot{Y}_{ij}(t)\cdot\Phi_{mn}dxdy + \iint \sum\sum G(\theta a_i^2 + b_j^2)\Phi_{ij}Y_{ij}\cdot\Phi_{mn}dxdy \\ = -\ddot{u}_0(t)\iint \rho\Phi_{mn}(x,y)\cdot dxdy\end{aligned} \tag{3.15}$$

Applying the orthogonality conditions and recalling Eq. (3.12), one obtains

$$\begin{aligned}\iint \rho\Phi_{mn}^2 dxdy\cdot\ddot{Y}_{mn}(t) + \iint \rho\Phi_{mn}^2 dxdy\cdot\omega_{mn}^2 Y_{mn}(t) \\ = -\ddot{u}_0(t)\iint \rho\Phi_{mn}(x,y)\cdot dxdy\end{aligned} \tag{3.16}$$

$$\ddot{Y}_{mn}(t) + \omega_{mn}^2\cdot Y_{mn}(t) = -\ddot{u}_0(t)\cdot\alpha_{mn} \tag{3.17}$$

where

$$\alpha_{mn} = \frac{\iint \rho \sin(a_m x)\cdot \sin(b_n y)dx\cdot dy}{\iint \rho \sin^2(a_m x)\cdot \sin^2(b_n y)dx\cdot dy}$$

$$\alpha_{mn} = \frac{16}{(2m-1)(2n-1)\pi^2} \tag{3.18}$$

Let $Y_{mn}(t) = \alpha_{mn} \cdot f_{mn}(t)$,

$$\ddot{f}_{mn}(t) + \omega_{mn}^2 \cdot f_{mn}(t) = -\ddot{u}_0(t) \tag{3.19}$$

For a damped forced vibration of the wall-soil system, a constant modal damping ratio λ is introduced (Seed and Idriss, 1967)

$$\ddot{f}_{mn}(t) + 2\lambda\omega_{mn} \cdot \dot{f}_{mn}(t) + \omega_{mn}^2 \cdot f_{mn}(t) = -\ddot{u}_0(t) \tag{3.20}$$

For a given ground excitation $\ddot{u}_0(t)$, a close-form solution of the system is found to be

$$u(x,y,t) = \sum\sum \sin a_m x \cdot \sin b_n y \cdot \alpha_{mn} \cdot f_{mn}(t) \tag{3.21}$$

where $f_{mn}(t)$ is the time history solution of Eq. (3.20) corresponding to a particular modal frequency ω_{mn}. It is noted that Eq. (3.20) is the standard damped vibration equation of a single degree of freedom system.

The dynamic earth pressure acting on the wall is the normal stress σ_x at x=0. The dynamic pressure distribution along the wall is

$$p(x,y,t)_{x=0} = \beta G \frac{\partial u}{\partial x}\Big|_{x=0}$$

$$p(x,y,t)_{x=0} = \beta G \sum\sum a_m \alpha_{mn} \cdot \sin(b_n y) \cdot f_{mn}(t) \qquad (3.22)$$

From Eq. 2.6, Eq. 2.10 and Eq. 2.14, the stress coefficient β for the different soil models is

For $v = 0$; $\beta = 2(1-v)/(1-2v)$

For $\sigma_y = 0$; $\beta = 2/(1-v)$

For the proposed method; $\beta = 2/(1-v)$

The total dynamic thrust acting on the wall is

$$P(t) = \int_0^H p(x,y,t)_{x=0} \cdot dy$$

$$P(t) = \beta G \cdot \sum\sum \frac{a_m \cdot \alpha_{mn}}{b_n} f_{mn}(t) \qquad (3.23)$$

$$P(t) = \beta G \cdot \sum\sum \frac{16 f_{mn}(t)}{(\pi^2 (2n-1)^2) L/H}.$$

The total dynamic moment acting at the base of the wall is

$$M(t) = \int_0^H y \cdot p(x, y, t)_{x=0} \cdot dy$$

$$M(t) = \beta G \cdot \sum\sum \frac{a_m \cdot \alpha_{mn} \cdot \sin(b_n H)}{b_n^2} f_{mn}(t) \tag{3.24}$$

For a harmonic input $\ddot{u}_0(t) = A_{max} \cdot e^{i\omega t}$, the amplitude of the steady state response $f_{mn}(t)$ is found from Eq. (3.20) to be

$$f_{mn} = \frac{A_{max}}{(\omega_{mn}^2 - \omega^2) + 2i \cdot \lambda \omega_{mn} \cdot \omega} \tag{3.25}$$

For any excitation $\ddot{u}_0(t)$ *the time history of the modal dynamic thrust* associated with a particular mode is obtained using Eq. (3.23). The time-history of the dynamic thrust for the desired number of modes is then determined by summation of the time histories of the modal dynamic thrusts.

For earthquake motion the peak modal thrust acting on the wall associated with a particular frequency ω_{mn} can be determined using the pseudo-spectral velocity S_v^{mn}. The pseudo-spectral velocity S_v^{mn} is derived from response spectral displacement S_d^{mn} by

$$S_v^{mn} = \omega_{mn} \cdot S_d^{mn} \tag{3.26}$$

where S_d^{mn} is also the peak $f_{mn}(t)$ corresponding to an excitation frequency ω_{mn}. From Eq. 3.23, the peak modal thrust P_{mn} is determined by

$$P_{mn} = \beta G \frac{a_m \cdot \alpha_{mm}}{b_n} \frac{S_v^{mn}}{\omega_{mn}} \tag{3.27}$$

The peak dynamic thrust is estimated by combining the individual peak modal thrusts by some approximate method. Either the absolute summation or the root square summation of the peak modal thrusts is commonly used.

Static 1g Solution: Validation of Model

In the previous chapter, three approximate models of the soil continuum were presented. The $v = 0$, $\sigma_y = 0$, and the proposed models were represented by different expressions for the coefficient θ in Eq. 2.5. It is necessary to examine the accuracy of the solutions given by each model. Wood's rigorous solution (Wood, 1973) will be used as the measure of the accuracy of the approximate solutions. Wood's solution is strictly valid for an elastic layer of finite length retained by a wall with a smooth interface at each end. Note that the "static" 1-g solution is the solution for very low frequencies.

From Eq. 3.25 the static deflection produced by a 1-g static force may be obtained by letting the exciting frequency ω approach zero.

$$f_{mn}(t) = \frac{g}{\omega_{mn}^2} \tag{3.28}$$

The corresponding 1-g static thrust is obtained by substituting Eq. 3.28 into Eq. 3.23

$$P_{st} = \rho\beta g \sum\sum \frac{a_m \cdot \alpha_{mn}}{b_n (b_n^2 + \theta a_m^2)} \tag{3.29a}$$

$$P_{st} = \rho\beta g \sum\sum \frac{16}{\pi (2n-1)^2 \omega_{mn}^2 \, L/H} \tag{3.29b}$$

The 1-g static moment acting at the base of the wall is

$$M_{st} = \rho\beta g \sum\sum \frac{a_m \cdot \alpha_{mn} \cdot \sin(b_n H)}{b_n^2 (b_n^2 + \theta a_m^2)} \tag{3.30}$$

The total thrust against the wall due to 1-g static horizontal force is determined by doing a double summation for modes m and n in Eq. 3.29. A normalized thrust ratio is defined as

$$\text{Thrust Ratio} = \frac{\text{Total Thrust}}{\rho H^2 \, A_{max}} \tag{3.31}$$

where A_{max} is the peak ground acceleration in m/sec^2, ft/sec^2 or other consistent units.

The three approximate models are used to obtain the total 1-g static force for two different wall-soil systems with L/H = 5.0 and L/H = 1.5.

Discussion of Results

The results of the analyses are compared with Wood's (1973) solutions for L/H = 5.0 and L/H = 1.5 are shown in Figs. 3.2(a) and 3.2(b), respectively. The following observations may be made

- For both L/H = 5.0 and L/H = 1.5 for all values of v, the proposed model gives results that are in very good agreement with the exact solutions. The model works better for walls retaining finite backfill (L/H = 1.5). The model gives a total force slightly less than the exact force.

- For L/H = 5.0, the $\sigma_y = 0$ model yields results that are in very good agreement with the exact solution for all v. For walls with long backfills, the accuracy of the $\sigma_y = 0$ model is comparable to that of the proposed model. The $\sigma_y = 0$ model overestimates the response by about 8%, the proposed model underestimates the response by about 5%.

- For L/H = 1.5, solutions by the proposed model are much closer to the exact solution for all values of v. The $\sigma_y = 0$ model overestimates the total force by up to 18%. The proposed model underestimates the total force by less than 4%.

- The v = 0 model gives good accuracy, provided values of $v < 0.3$. As v exceeds 0.3, the solutions start to deviate from the exact solutions. For L/H = 5.0, the accuracy of the solution becomes unacceptable as $v > 0.4$.

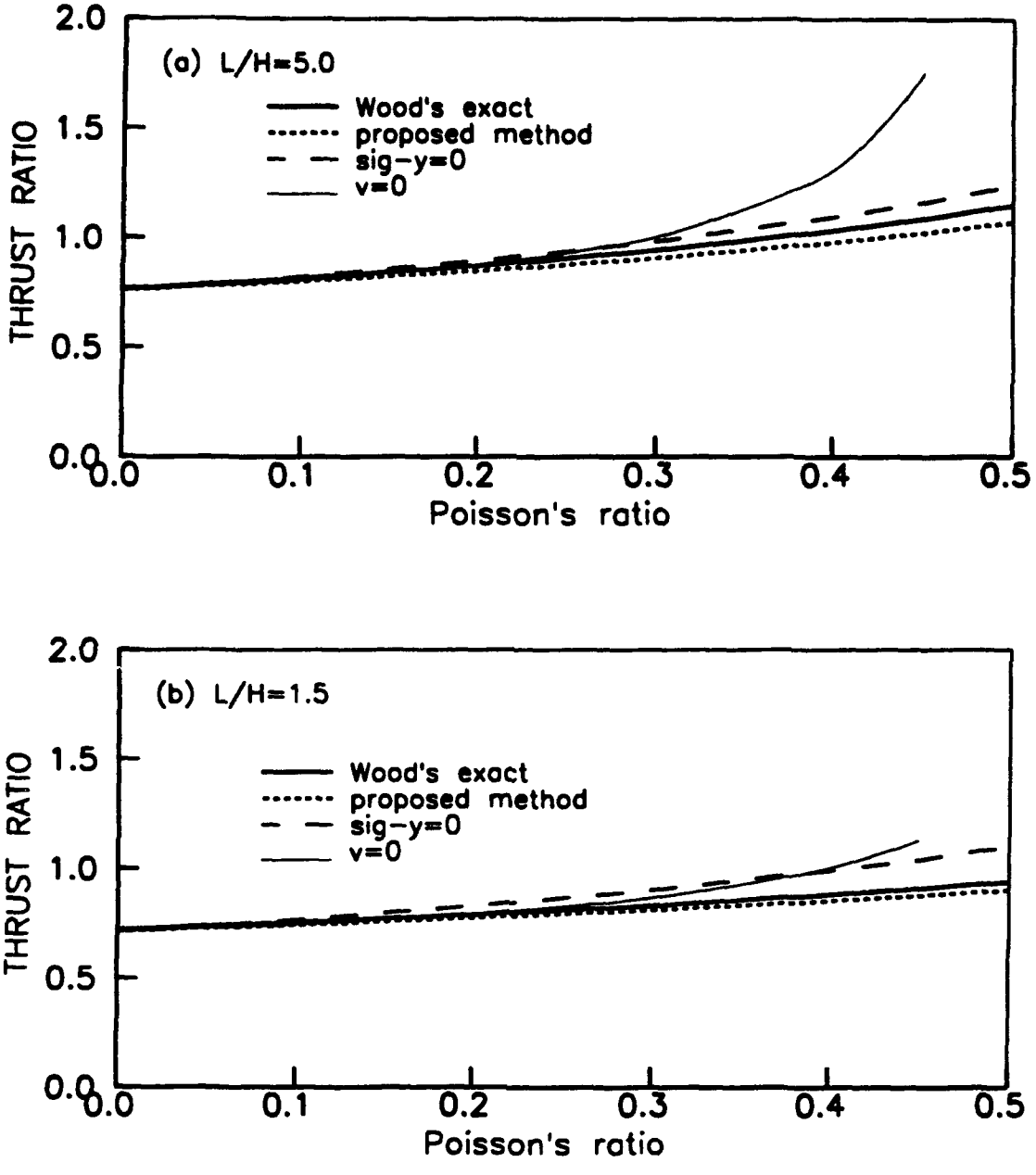

Fig. 3.2: Comparison of approximate solutions for rigid-wall systems with Wood's (1973) exact solution for (a) L/H=5.0 and (b) L/H=1.5.

Recently, Veletsos and Younan (1994) also evaluated the accuracy of the $\sigma_y = 0$ and $\nu = 0$ models compared to Wood's rigorous solution. Their findings regarding these models agree with those above. However, these more recent studies were limited to semi-infinite backfills.

The studies indicate that the proposed model gives the best approximation of solutions for the rigid-wall systems with elastic backfills. Therefore, this proposed model will be used for all further studies.

CHAPTER 4

ELASTIC DYNAMIC RESPONSE OF PILES

Equations of Motion for Soil-Pile System

The simplified model of the soil continuum derived earlier is now extended to incorporate the important aspects of 3-D response and adapted to accommodate piles.

Under vertically propagating shear waves the soils mainly undergo shear deformations in horizontal planes except in the area near the pile where extensive compressive deformations develop in the direction of shaking. The compressive deformations also generate additional shearing deformations along the sides of the pile because of the limited extent of the pile cross-section. In light of these observations, assumptions are made that dynamic motions of soils are governed by two kinds of shear stresses, and compressive stresses in the direction of shaking, y.

Let v represent the horizontal displacement of the soil in the direction of shaking, y (Fig. 4.1). The inertial force is $\rho_s \frac{\partial^2 u}{\partial t^2}$. The compressive force in the direction of shaking is $\theta G \frac{\partial^2 v}{\partial y^2}$. The shear waves propagate in the z direction. The shear force in the xOy plane is $G \frac{\partial^2 v}{\partial x^2}$, and the shear force in yOz plane is $G \frac{\partial^2 v}{\partial x^2}$. Applying dynamic equilibrium in the y-direction, the dynamic governing equation under free vibration of the soil continuum is written as

$$G \frac{\partial^2 v}{\partial x^2} + \theta G \frac{\partial^2 v}{\partial y^2} + G \frac{\partial^2 v}{\partial z^2} = \rho_s \frac{\partial^2 v}{\partial t^2} \qquad (4.1)$$

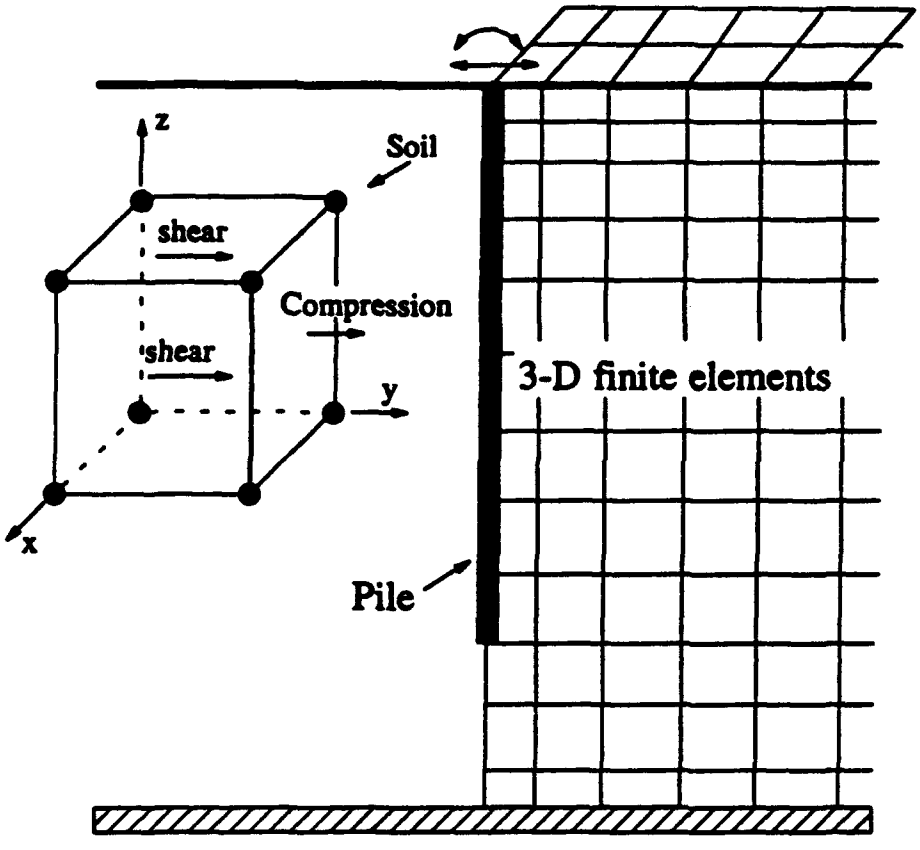

Fig. 4.1. Important aspects of pile-soil interaction during horizontal excitation by shear waves.

where $\theta = 2/(1-\nu)$, G is the complex shear modulus, and ρ_s is the mass density. Since soil is a hysteretic material, the complex shear modulus G is expressed as $G = G_0 (1+i\,2\lambda)$, in which G_0 is the shear modulus of soil, and λ is the equivalent viscous damping ratio. Radiation damping will be considered later.

Piles are modelled using ordinary Eulerian beam theory. Only the bending moment in the plane of shaking (yOz) is included. This consideration is appropriate in the case of earthquake loading for single piles.

The dynamic equation of motion for a vertical pile is written as

$$E_p I_y \frac{\partial^4 v}{\partial z^2} = \rho_p \frac{\partial^2 v}{\partial t^2} \tag{4.2}$$

where E_pI_y is the flexural rigidity of the pile in the direction of shaking, and ρ_p is the mass density of the pile.

Finite Element Formulation of Equations of Motion

The 3-dimensional soil continuum is divided into a number of 3-D finite elements of the type shown in Fig. 4.2. The displacement field at any point in each element is specified by the nodal displacements and appropriate shape functions. A linear displacement field in the soil element is used because of its simplicity and effectiveness.

The displacement vector v(x,y,z) is expressed as

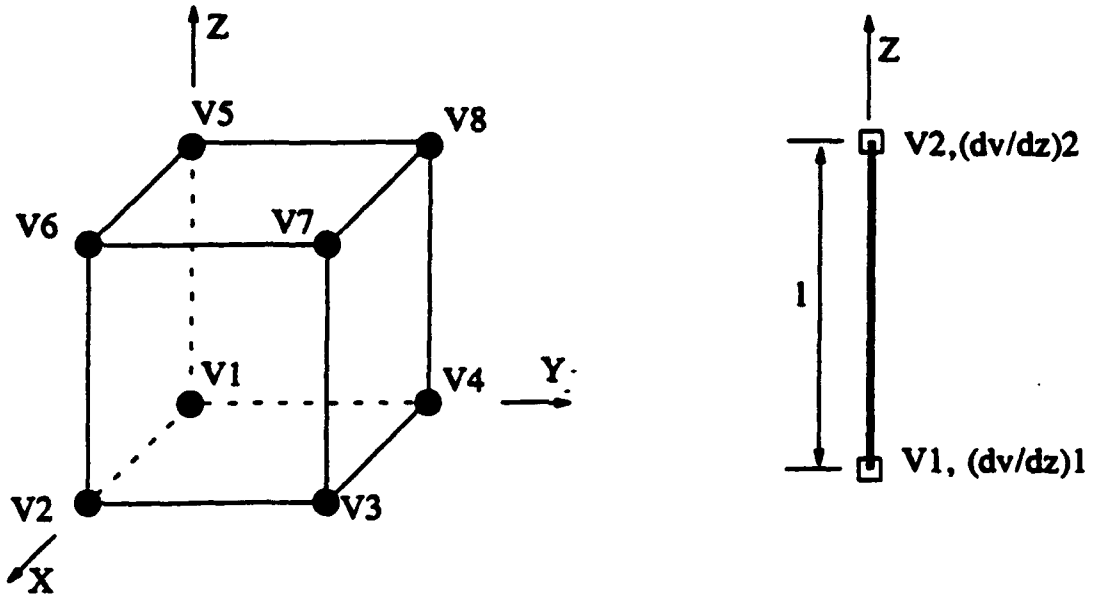

Fig. 4.2: Finite elements used for soil continuum and pile.

$$v(x,y,z) = \Sigma N_i \times v_i, \ldots i = 1,8 \qquad (4.3)$$

where N_i is a shape function, and v_i is a nodal displacement.

Applying the Galerkin's weighted residual procedure to Eq. 4.1, the complex valued stiffness matrix of the soil element is determined

$$[K]_{soil} = \iint \left(\theta G \frac{\partial N_i}{\partial y} \frac{\partial N_j}{\partial y} + G \frac{\partial N_i}{\partial x} \frac{\partial N_j}{\partial x} + G \frac{\partial N_i}{\partial z} \frac{\partial N_j}{\partial z} \right) dxdydz \qquad (4.4)$$

For a vertical beam element, (Fig. 4.2) the stiffness matrix is

$$[K]_{pile} = \frac{E_p I_y}{\ell^3} \begin{bmatrix} 12 & 6\ell & -12 & 6\ell \\ 6\ell & 4\ell^2 & -6\ell & 2\ell^2 \\ -12 & -6\ell & 12 & -6\ell \\ 6\ell & 2\ell^2 & -6\ell & 4\ell^2 \end{bmatrix} \qquad (4.5)$$

The two nodes in a vertical beam element are shared by adjacent soil elements, thus coupling the pile and the soil. The stiffness of a node, therefore, is comprised of stiffness contributions from both the pile and the soil.

Consistent mass matrices are used for both soil elements and pile elements. The consistent mass matrix for a soil element is

$$[M]_{soil} = \iint \rho_s \cdot N_i N_j \cdot dxdydz \qquad (4.6)$$

The consistent mass matrix for a pile element is written as

$$[M]_{pile} = \frac{\rho_p A \ell}{420} \begin{bmatrix} 156 & 22\ell & 54 & -13\ell \\ 22\ell & 4\ell^2 & 13\ell & -3\ell^2 \\ 54 & 13\ell & 156 & -22\ell \\ -13\ell & -3\ell^2 & -22\ell & 4\ell^2 \end{bmatrix} \qquad (4.7)$$

The global stiffness matrix [K] and the global mass matrix [M] are constructed by standard routines.

The radiation damping is modelled by using a set of set of dashpots along the pile shaft. The damping force F_d per unit length along the pile is considered proportional to the velocity and is given by

$$F_d = c_r \cdot \frac{\partial v}{\partial t} \tag{4.8}$$

where

$$c_r = 6\rho_s V_s d\, a_0^{-0.25} \tag{4.9}$$

where c_r is the radiation dashpot coefficient.

Gazetas et al. (1993) proposed simple expressions for the radiation dashpot coefficients c_r for both horizontal motion and vertical motion. The element radiation damping matrix $[C]_{elem}$ is

$$[C]_{elem} = \frac{c_r \ell}{420}\begin{bmatrix} 156 & 22\ell & 54 & -13\ell \\ 22\ell & 4\ell^2 & 13\ell & -3\ell^2 \\ 54 & 13\ell & 156 & -22\ell \\ -13\ell & -3\ell^2 & -22\ell & 4\ell^2 \end{bmatrix} \tag{4.10}$$

The global dynamic equilibrium equation in matrix form is now

$$[M]\{\ddot{v}\} + [C]\{\dot{v}\} + [K]\{v\} = \{P(t)\} \tag{4.11}$$

in which $\{\ddot{v}\}$, $\{\dot{v}\}$ and $\{v\}$ are the nodal accelerations, velocities and displacements, respectively, and $\{P(t)\}$ are external dynamic loads.

Solutions of Eq. 4.10 will now be developed to give the stiffness and damping of single piles (pile impedances) as a function of frequency. These impedances will be compared with impedances calculated using the full 3-D equations for the continuum to verify the accuracy of the proposed model for pile analysis.

CHAPTER 5

PILE IMPEDANCES: SOLUTIONS FOR HARMONIC LOADING

The impedance K_{ij} are defined as the amplitudes of harmonic forces (or moments) that have to be applied at the pile head in order to generate a harmonic motion with a unit amplitude in the direction of the specified degree of freedom (Novak, 1991) as shown in Fig. 5.1.

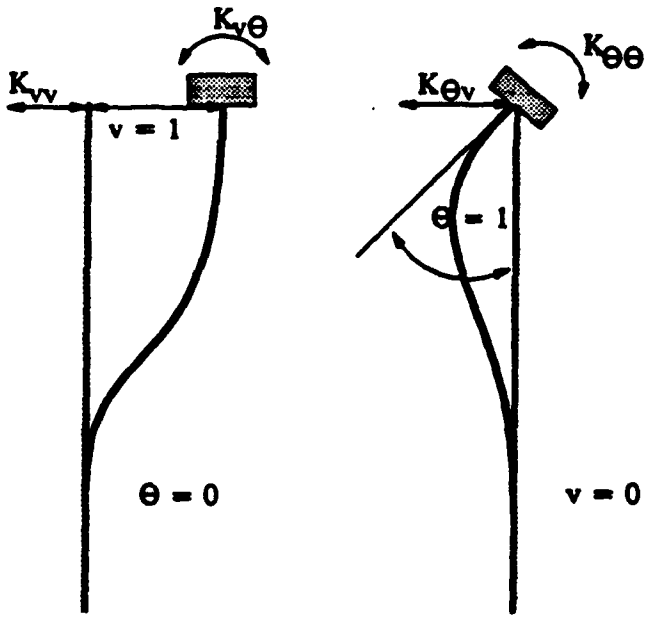

Fig. 5.1: Pile head impedances.

The impedances are defined as follows:

K_w: the complex-valued pile head horizontal force required to generate unit horizontal displacement (u=1.0) at the pile head while the pile head rotation is fixed (θ=0).

$K_{v\theta}$: the complex-valued pile head moment generated by the unit lateral displacement (u=1.0) at the pile head while the pile head rotation is fixed (θ=0)

$K_{\theta\theta}$: the complex-valued pile head moment required to generate the unit pile head rotation (θ=1.0) while pile head lateral displacement is fixed (u=0)

Since the pile head impedances K_{vv}, $K_{v\theta}$, $K_{\theta\theta}$ are complex valued, they are usually expressed by their real and imaginary parts as

$$K_{ij} = k_{ij} + i \cdot C_{ij} = k_{ij} + i \cdot \omega c_{ij} \tag{5.1}$$

in which k_{ij} and C_{ij} are the real and imaginary parts of the complex impedance, respectively, and are usually referred as the stiffness and damping at the pile head. $i = \sqrt{-1}$; $c_{ij} = C_{ij} / \omega$ = coefficient of equivalent viscous damping; and ω is the circular frequency of the applied load. All the parameters in Eq. 5.1 are dependent on frequency ω. Determination of the pile impedances requires solutions of the equations of motion for harmonic loading.

Under harmonic loading $P(t) = P_0 e^{i\omega t}$, the displacement vector is of the form $v = v_0 e^{i\omega t}$, and Eq. 4.11 is rewritten as

$$\left\{[K] + i \cdot \omega[C] - \omega^2[M]\right\} \{v_0\} = \{P_0\} \tag{5.2}$$

or

$$[K]_{global} \{v_0\} = \{P_0\} \tag{5.3}$$

where

$$[K]_{global} = [K] + i \cdot \omega[C] - \omega^2[M] \tag{5.4}$$

The pile head impedances K_{vv}, $K_{v\theta}$ and $K_{\theta\theta}$ can be obtained using Eq. 4.8 by applying appropriate loading and fixity conditions at the pile head.

Determination of Impedances K_{vv} and $K_{v\theta}$

If the pile head is fixed against rotation and a unit horizontal displacement applied at the pile head, then Eq. 5.3 has the form

$$[K]_{global} \begin{Bmatrix} v_0^A \\ 1.0 \\ 0.0 \end{Bmatrix} = \begin{Bmatrix} 0 \\ K_{vv} \\ K_{u\theta} \end{Bmatrix} \tag{5.5}$$

where v_o^A are the displacements of the nodes other than pile head. Eq. 5.5 can be solved by dividing the equation by K_{vv} and eliminating the row corresponding to zero rotation

$$K]_{global} \begin{Bmatrix} v_o^A / K_{vv} \\ v_o^p \end{Bmatrix} = \begin{Bmatrix} 0 \\ 1.0 \end{Bmatrix} \tag{5.6}$$

This equation suggests that an easier alternative for determining impedances is to apply a unit horizontal force at the pile head and calculate the complex displacement v_0^P. The moment at pile head M_0^P corresponding to v_0^P is also calculated.

Then the pile head impedance K_{vv} is determined by

$$K_{vv} = \frac{1.0}{v_o^p} \tag{5.7}$$

and the corresponding cross-impedance

$$K_{v\theta} = \frac{M_o^p}{v_o^p} \tag{5.8}$$

Determination of Rotational Impedance $K_{\theta\theta}$

For a pile head fixed against horizontal displacement and given a unit pile head rotation Eq. 5.3 has the form

$$K]_{global} \begin{Bmatrix} v_0^B \\ 1.0 \\ 0.0 \end{Bmatrix} = \begin{Bmatrix} 0 \\ K_{\theta v} \\ K_{\theta\theta} \end{Bmatrix} \tag{5.9}$$

or

$$[K]_{global} \begin{Bmatrix} v_0^B / K_{\theta\theta} \\ \theta_0^p \end{Bmatrix} = \begin{Bmatrix} 0 \\ 1.0 \end{Bmatrix} \tag{5.10}$$

where v_0^B are the displacements of nodes other than pile head. The pile head rotation θ_0^p is the complex response to the application of a unit moment at the pile head.

The rotational impedance $K_{\theta\theta}$ is then given as

$$K_{\theta\theta} = \frac{1.0}{\theta_o^p} \tag{5.11}$$

Because of reciprocity principle, the cross-coupling impedances $K_{v\theta}$ and $K_{\theta v}$ are identical.

Dynamic Impedance of Single Piles

Analyses are conducted to determine the frequency dependence of the impedances K_{vv}, $K_{v\theta}$ and $K_{\theta\theta}$ for single piles. The dimensionless frequency ratio a_0, is used to characterize the frequency, where a_0 is defined by

$$a_o = \frac{\omega d}{V_s} \tag{5.12}$$

in which ω is the angular frequency of the exciting loads (force or moment) at the pile head, d is the diameter of the pile, and V_s is the shear wave velocity of the soil medium. For a uniform soil profile with a shear modulus G and a mass density ρ, $V_s = \sqrt{G/\rho}$.

For given values of E_p/E_s and a_0, the ratios $K_{vv}/(E_s d)$, $K_{v\theta}/(E_s d^2)$, and $K_{\theta\theta}/(E_s d^3)$, remain constant as the soil modulus E_s varies if the soil profile is uniform. Therefore the normalized impedances $K_{vv}/E_s d)$, $K_{v\theta}/(E_s d^2)$, and $K_{\theta\theta}/(E_s d^3)$ are used in presenting the frequency dependence of the impedances.

To assess the accuracy of the proposed simplified 3-D finite element approach, the impedance functions of the pile-soil system shown in Fig. 5.2 were computed over a range of frequencies and compared with the full 3-D linear elastic solutions of Kaynia and Kausel (1982). However, the latter solutions, though regarded as benchmark solutions, are not exact. They assume the form of the pressure distribution between soil and pile at any elevation to be uniform around the laterally displacing pile.

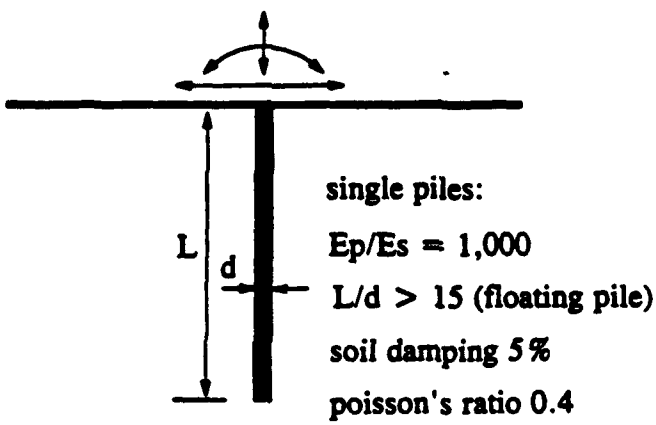

Fig. 5.2: A pile-soil system used for computing impedance functions.

The impedances are determined for $E_p/E_s = 1{,}000$, Poisson's ratio $\nu = 0.4$, and a damping ratio $\lambda = 5\%$.

The finite element mesh shown in Fig. 5.3 is used for the analysis. The heavy dark vertical element is the pile. Because of the symmetric character of the problem, only half of the full mesh is required to model the response of pile-soil interaction. The half mesh consists of 1463 nodes

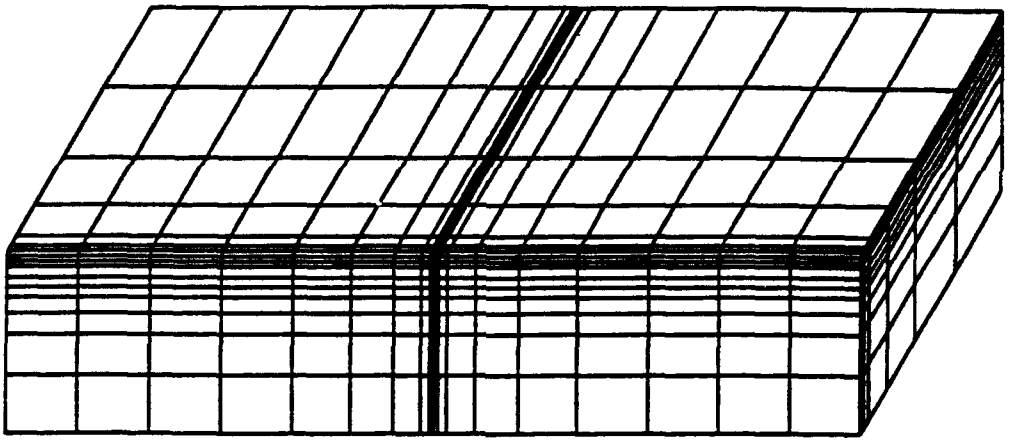

Fig. 5.3: Finite element modelling of single pile for computing impedance.

and 1089 elements. The use of symmetry reduces the size of the global matrix by a factor of 4.0 and greatly reduces the computational time. The computing time is 300 seconds for each frequency using a 33 Hz 486 PC computer.

The half-mesh includes only half the pile so that for the linear beam element E_p and ρ_p must be reduced by a factor of 2. The loads applied to the pile must also be reduced from 1.0 to 0.5. The effects of these reductions must be kept in mind when the corresponding impedances are calculated.

Discussion of Results

Since the normalized impedances are complex quantities, they are given in terms of their real (stiffness) and imaginary (damping) parts. The computed normalized stiffnesses and damping ratios as functions of dimensionless frequency a_0 are compared with the solutions of Kaynia and Kausel (1982) in Figs. 5.4, 5.5 and 5.6.

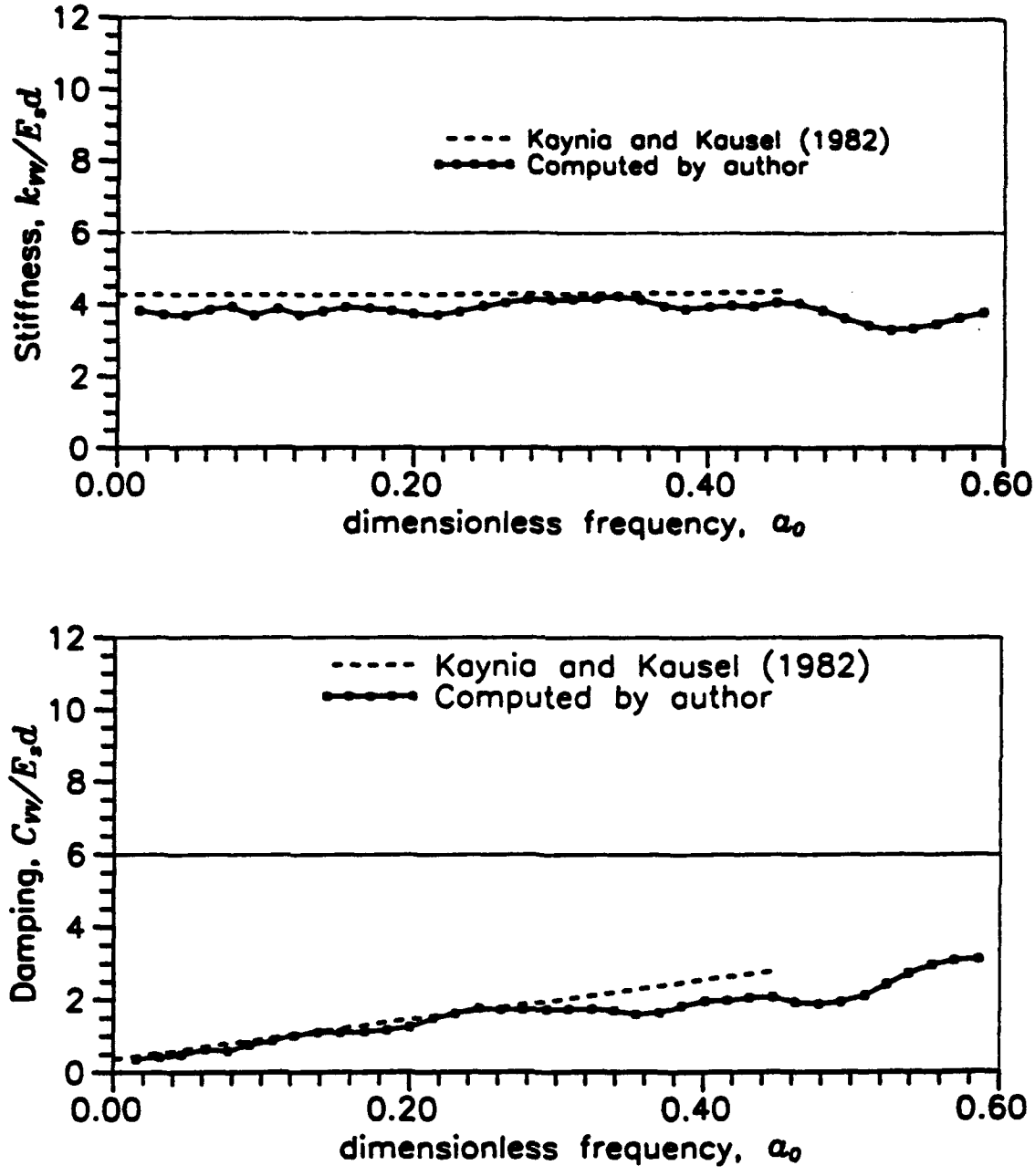

Fig. 5.4: Normalized stiffness k_{vv} and damping C_{vv} versus a_0 for single piles ($E_p/E_s = 1000$, $\nu = 0.4$, $\lambda = 5\%$).

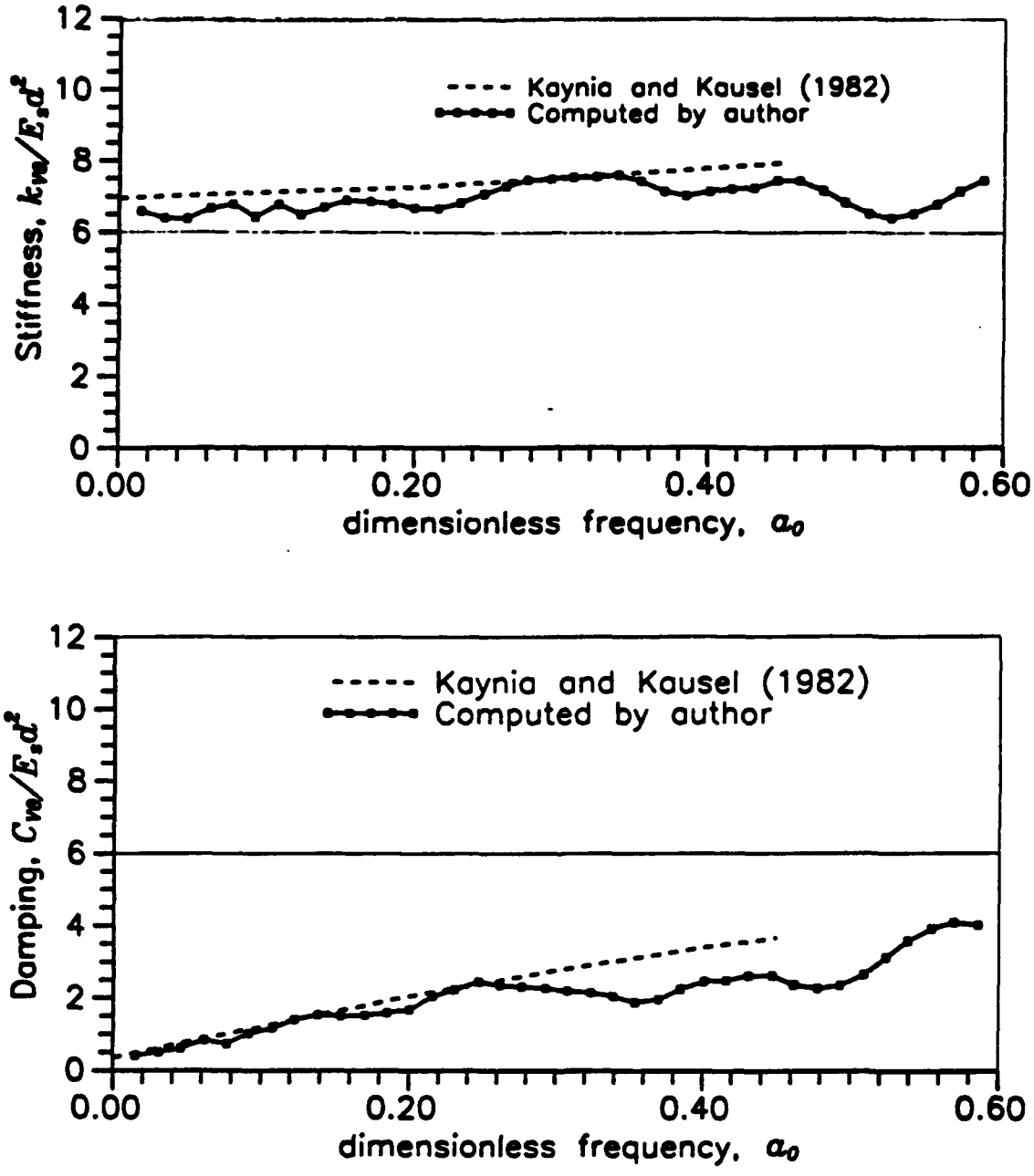

Fig. 5.5: Normalized stiffness k_{v0} and damping C_{v0} versus a_0 for single piles ($E_p/E_s = 1000$, $\nu = 0.4$, $\lambda = 5\%$).

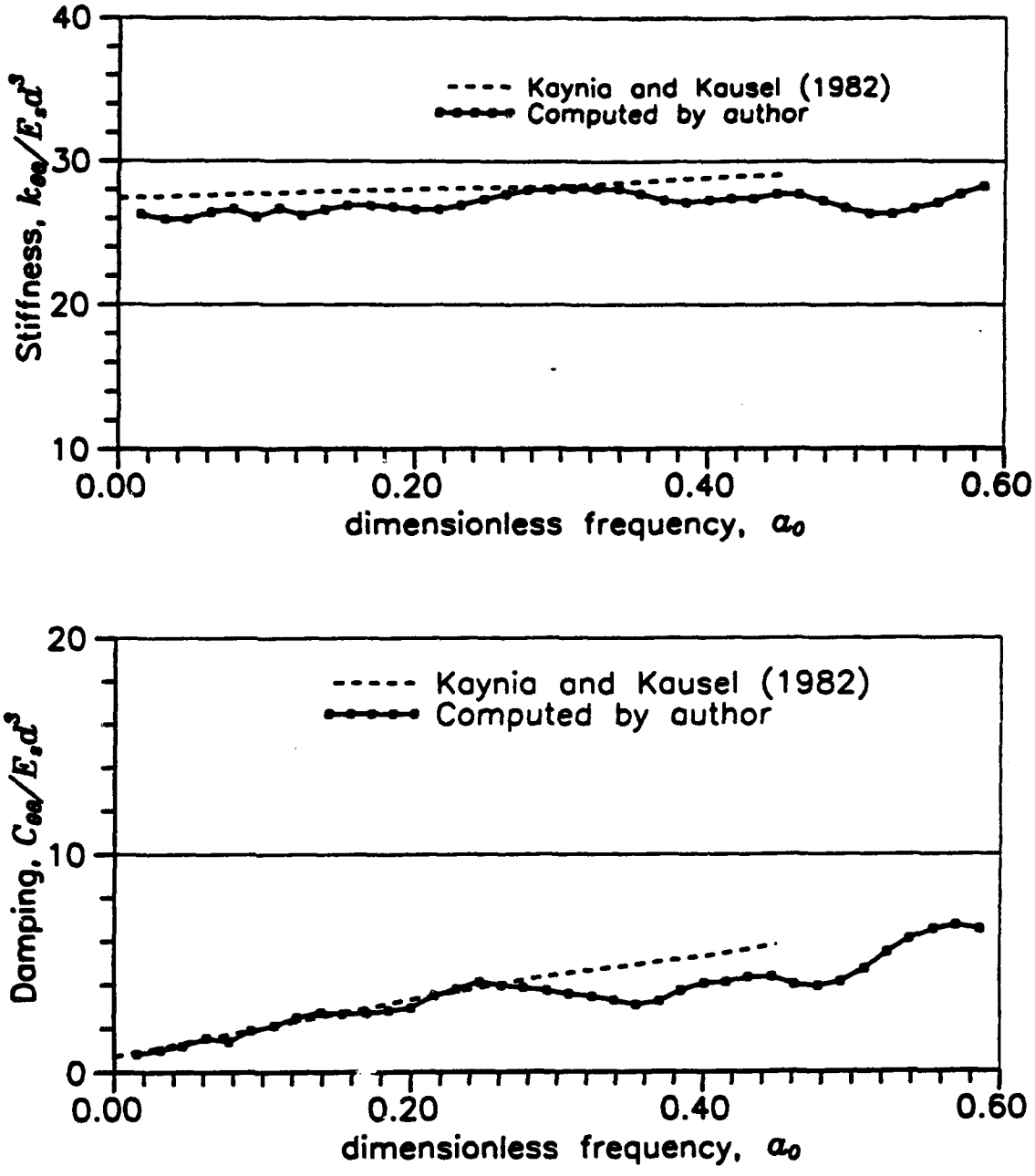

Fig. 5.6: Normalized stiffness $k_{\theta\theta}$ and damping $C_{\theta\theta}$ versus a_0 for single piles ($E_p/E_s = 1000$, $\nu = 0.4$, $\lambda = 5\%$).

In general, the impedances computed by the simplified method agree well with those of Kaynia and Kausel (1982). The horizontal stiffnesses k_{vv} computed by Kaynia and Kausel (1992) are about 10% larger than those computed using the simplified model. The other two stiffnesses $k_{v\theta}$ and $k_{\theta\theta}$ show closer agreement. The differences are on the average about 5%.

It is hard to decide which of the two solutions represents more closely the true solution of this problem because both were obtained by approximate methods. In Kaynia and Kausel's solution the horizontal load applied to soil medium by the pile is assumed uniformly distributed on the cylindrical soil surface around the pile. This does not model well the non-uniform distribution of lateral pressure on the cylindrical surface of the surrounding soil caused by the laterally deflecting pile

The size and number of the finite elements affect the computed value of the impedance. The accuracy increases as the number of finite elements increases especially as the frequency increases. At high frequencies (such as $a_0 > 0.4$), large numbers of finite elements are needed to capture the number of modes that are significant for response at that frequency.

Figure 5.7 shows a comparison of the dynamic stiffnesses computed by two different meshes. It is clear that mesh size becomes significant when the frequency becomes high. A finer mesh is needed to represent the dynamic responses accurately.

For earthquake loading, the non-dimensional frequency for pile foundations is usually less than $a_o = 0.3$ for the important frequencies in the ground motions. In this frequency range, the approximate method proposed is very accurate, even with a rather coarse mesh.

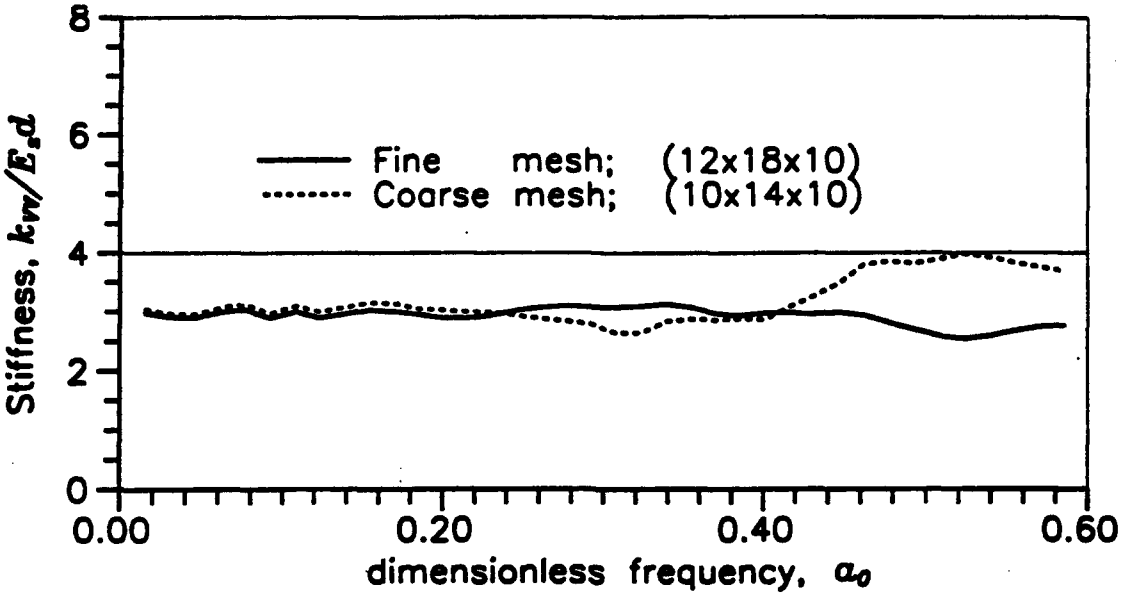

Fig. 5.7: Effects of mesh size on stiffness.

CHAPTER 6

NONLINEAR DYNAMIC RESPONSE ANALYSIS OF PILES

The equations of motion are given by the incremental form of Eq. 4.8 as

$$M]\{\Delta\ddot{v}\}+[C]\{\Delta\dot{v}\}+[K]\{v\} = \{P(t)\} = -[M][I]\,\Delta\ddot{v}_b(t) \qquad (6.1)$$

Analysis of nonlinear response must be conducted in the time domain. The direct step by step integration procedure developed by Wilson et al. (1973) is used to integrate the equations of motion.

Rayleigh damping is used to model the hysteretic damping of the soil for nonlinear analysis. The damping element matrix is given by

$$[C]_{elem} = \alpha[M]_{elem} + \beta[K]_{elem} \qquad (6.2)$$

in which α and β are constants related to the viscous damping ratio for the element. Let

$$\alpha = \lambda_{elem} / \omega_1 \quad \text{and} \quad \beta = \lambda_{elem} / \omega_1 \qquad (6.3)$$

where λ_{elem} is the damping ratio corresponding to element shear strainand ω_1 is the fundamental frequency of the system (Idriss et al., 1974).

The global damping matrix [C] is the aggregate of all the element damping ratios and the radiation damping elements along the pile.

For nonlinear analysis because of integration in the time domain, it is more efficient to use a diagonal mass matrix rather than the consistent mass matrix used earlier for harmonic analysis. Therefore, the mass matrices for soil and beam elements, $[M]_{soil}$ and $[M]_{beam}$, respectively, are given by

$$[M]_{soil} = \frac{\rho_s \cdot vol}{8} \{1.0, 1.0, 1.0, 1.0, 1.0, 1.0, 1.0, 1.0\} \tag{6.4}$$

and

$$M]_{beam} = \rho_p \, A\ell \, \{1/2, 1/78, 1/2, 1/78\} \tag{6.5}$$

Soil modulus and damping in soils are shear strain dependent (Seed and Idriss, 1970). During analysis compatibility is maintained between the computed shear strains and the effective modulus and damping in each finite element. The compatibility can be restored for each time increment during integration of the equations of motion or at specified times which are multiples of the time increment for integration. This procedure differs from the equivalent linear method used in programs such as SHAKE (Schnabel et al., 1972) in which compatibility is enforced only after the complete response analysis has been completed. Ensuring final compatibility in that case requires iterative analysis using the entire duration of the earthquake in each analysis. No iterative analyses are required when compatibility is enforced during the analysis.

Two other features distinguish the nonlinear model proposed here from the Schnabel et al. (1972) model. Shear yielding is incorporated by introducing a very low modulus when the strength of the soil is reached. No tensile stresses are allowed. This is accomplished by

introducing a very low modulus when the normal stress in any direction tends to become greater than the tensile strength of the soil if any.

The nonlinear method of analysis will be validated now using data from strong shaking tests of a single pile in a centrifuge.

CHAPTER 7

CENTRIFUGE TESTS ON A SINGLE PILE UNDER STRONG SHAKING

Test Set-Up

The nonlinear method is used to analyze the seismic response of a single pile in a centrifuge test which was carried out on the California Institute of Technology (Caltech) centrifuge by B. Gohl (1991). Details of the test may also be found in a paper by Finn and Gohl (1987). Fig. 7.1 shows the soil-pile-structure system used in the test. A 209.5 mm long stainless steel tube pile having an outside diameter of 9.52 mm and a wall thickness of 0.25 mm is embedded in a dry loose sand foundation. The model pile is instrumented by 8 pairs of foil type strain gauges mounted on the outside of the pile to measure bending strains at the locations shown in Fig. 7.1. An average centrifuge acceleration of 60g was used in the tests.

The pile has a free standing length of 16.5 mm above the soil surface. The effect of a super-structure is simulated by clamping a rigid mass to the head of the pile. The weight of the structural mass including the pile head insert and the pile head clamp is 2.416 N. The mass moment of inertia about the centre of gravity is $I_{cg} = 0.0683$ N.sec^2.mm. The centre of gravity of the mass is located 16.5 mm above the pile head. The model pile has an average flexural rigidity of 13.26 N.m^2 and a mass density of 74.7 kN/m^3.

The pile head mass is instrumented using a non-contact photovoltaic displacement transducer and an Entran miniature accelerometer. The locations of the accelerometer and light emitting diode (L.E.D.) used by the displacement sensor are shown in Fig. 7.1. The pile head displacements are measured with respect to the moving base of the soil container.

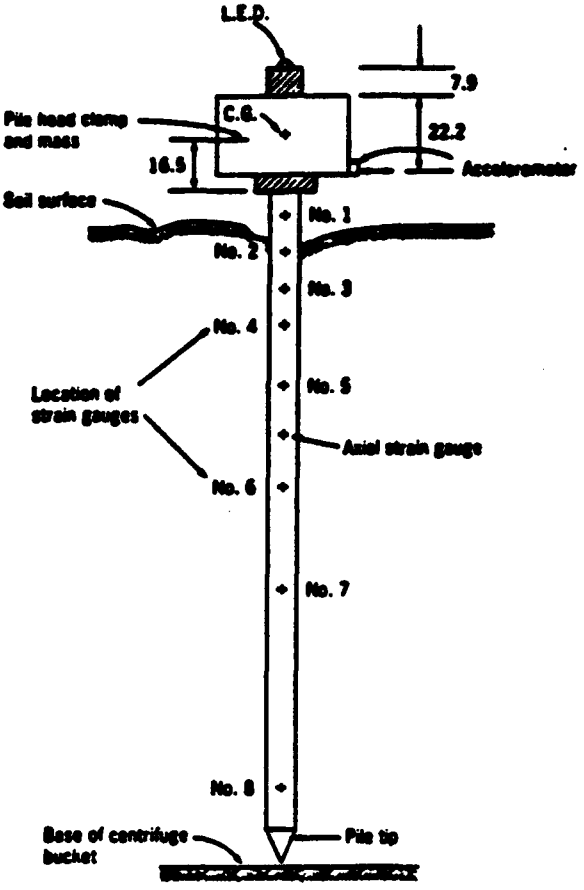

Fig. 7.1. The layout of the centrifuge test for a single pile.

The sand used for the test was a loose sand with a void ratio $e_o = 0.78$ and a mass density $\rho = 1.50$ Mg/m^3. Gohl (1991) has shown that the low strain shear moduli of the sand foundation vary as the square root of the depth, and they can be quantitatively evaluated using the Hardin and Black (1968) Eq. (7.1)

$$G_{max} = 3230 \frac{(2.973 - e_o)^2}{1 + e_o} (\sigma'_m)^{0.5} \qquad (7.1)$$

where e_o is the in-situ void ratio of the sand and σ'_m is the mean normal effective confining pressure in kPa.

A horizontal acceleration is input at the base of the system. The peak acceleration of the input motion is 0.158g. The computed Fourier amplitude ratios of the pile head response and the free field motion with respect to the input motions are given in Fig. 7.2(a) and Fig. 7.2(b). The natural frequency of the free field acceleration is estimated to be 2.75 Hz from Fig. 7.2(b) and the

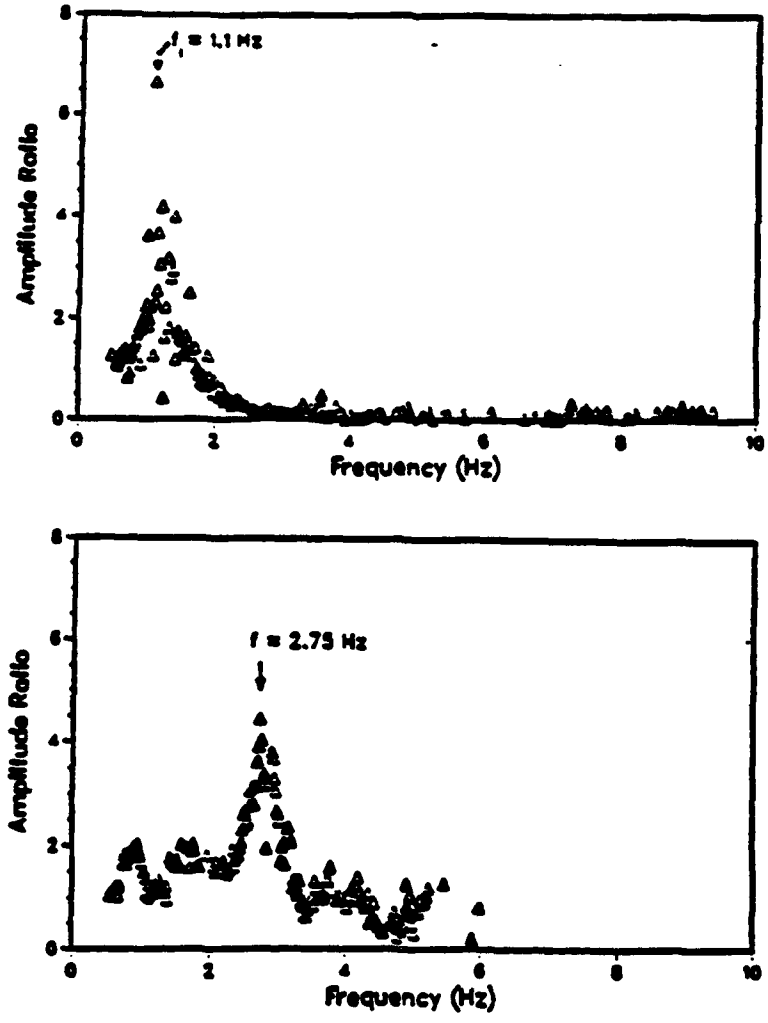

Fig. 7.2. The Fourier Spectra of accelerations (after Gohl, 1991).

fundamental frequency of the pile (from Fig. 7.2(a)) to be 1.1 Hz. The period of peak pile response is much longer than the period of the free field.

The centrifuge test was analyzed by the simplified 3-D finite element method of analysis. Fig. 7.3 shows the finite element model used for analysis. The sand deposit is divided into 11 layers. Layer thickness is reduced as the soil surface is approached to allow more detailed modelling of the stress and strain field where lateral soil-pile interaction is strongest. The pile is modelled using 15 beam elements including 5 elements above the soil surface. The super-structure mass is treated as a rigid body.

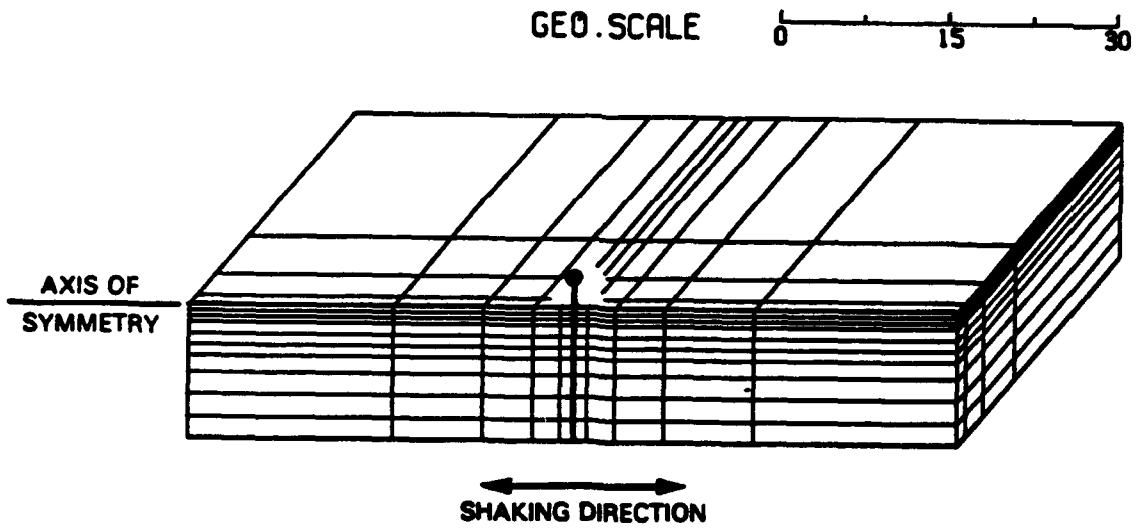

Fig. 7.3. The finite element modelling of centrifuge test.

The finite element analysis is carried out in the time domain. Nonlinear analysis is performed to account for the changes in shear moduli and damping ratios due to dynamic shear strains. The shear-strain dependency of both the shear modulus and damping ratio used in the analysis is shown in Fig. 7.4. The low strain shear moduli G_{max} were determined using Eq. (7.1).

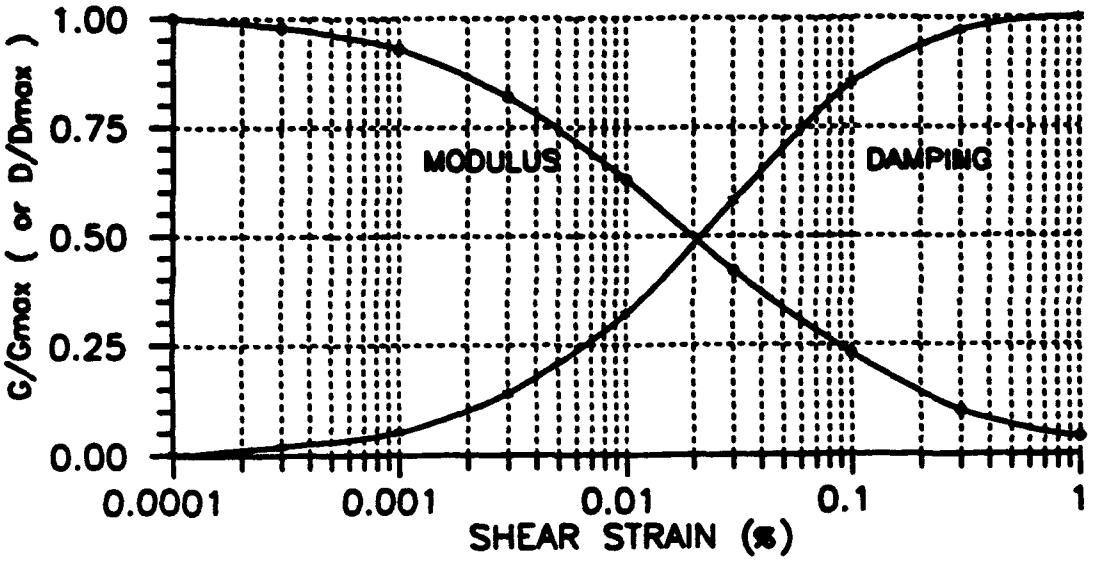

Fig. 7.4. The relationships between shear modulus, damping and the shear strain.

Discussion of Results

The computed acceleration response at the pile head is plotted against the measured response in Fig. 7.5. Fairly good agreement between the measured and the computed accelerations is observed in the region of strong shaking.

The computed time histories of moments in the pile at the ground surface and at a depth of 3 m are plotted against the corresponding recorded time histories in Fig. 7.6 and Fig. 7.7. There is satisfactory agreement between the computed and measured moments in the range of larger moments. The computed and measured moment distributions along the pile at the moment of peak pile head deflection are shown in Fig. 7.8. The computed moments agree quite well with the measured moments. The moments increase to a maximum value at a depth of 3.5 diameters, and

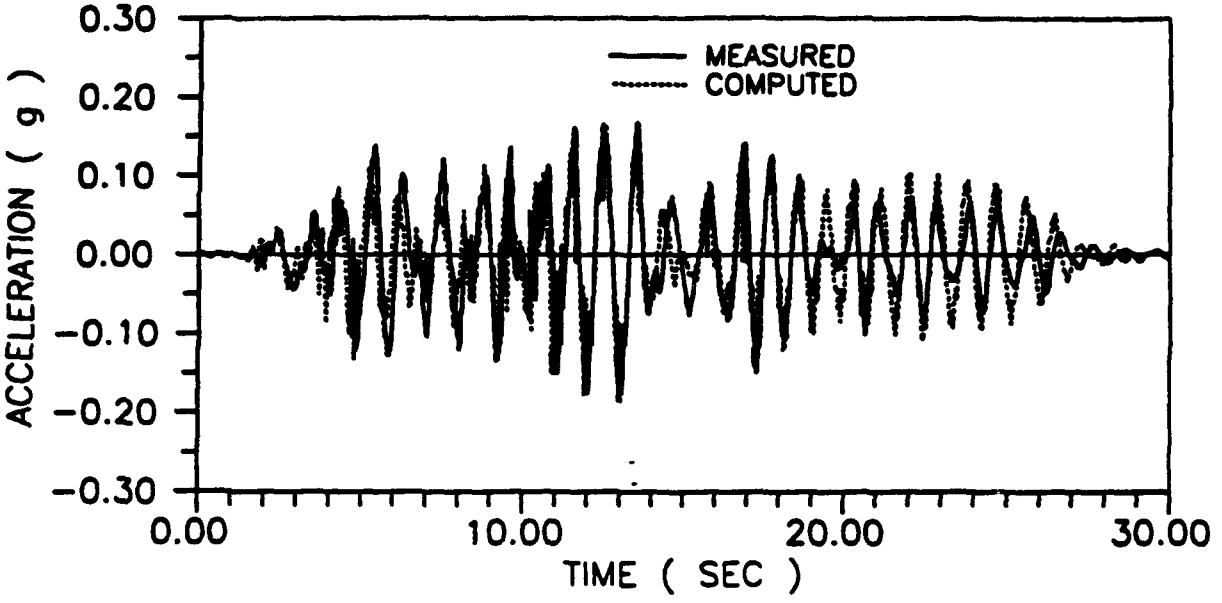

Fig. 7.5. The computed versus measured acceleration response at the pile head.

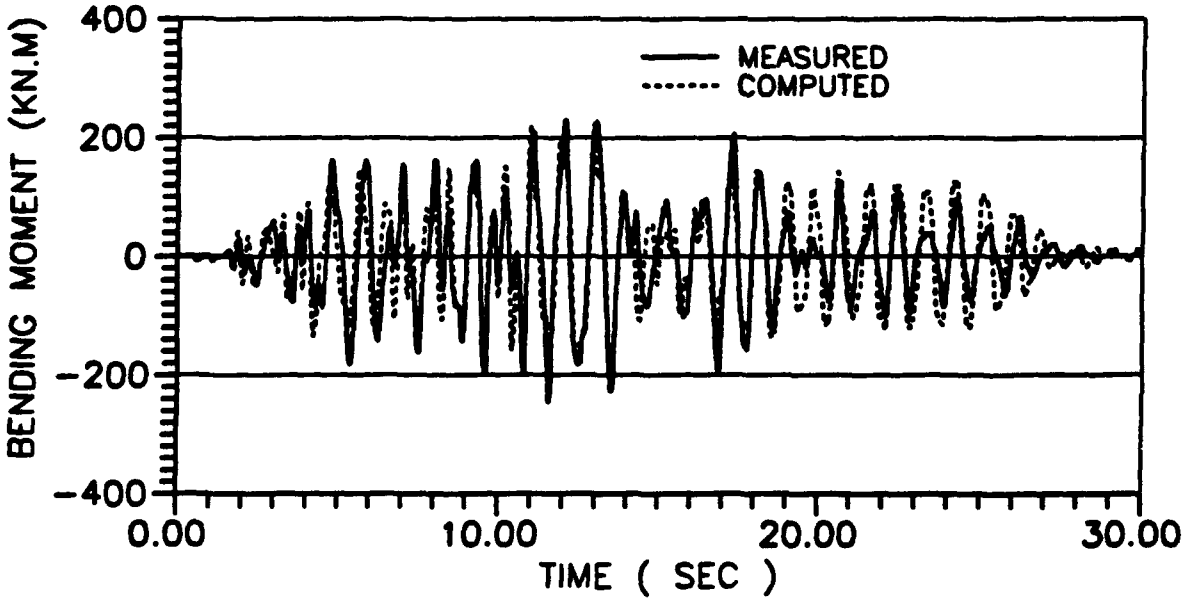

Fig. 7.6. The computed versus measured moment response in the pile at the ground surface.

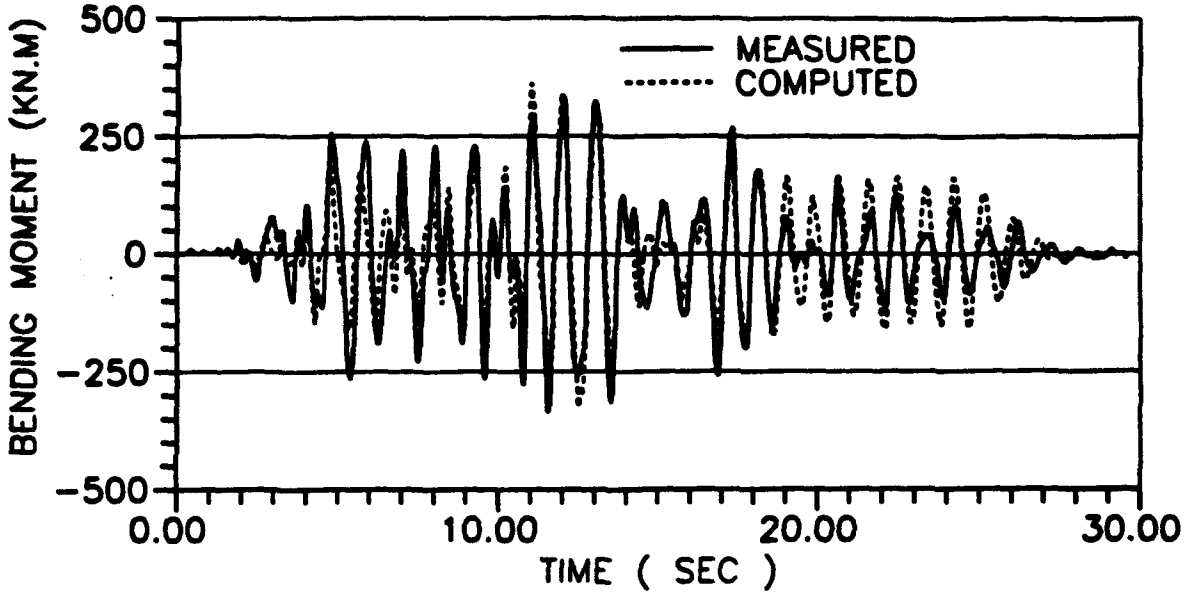

Fig. 7.7. The computed versus measured moment response at depth D = 3 m.

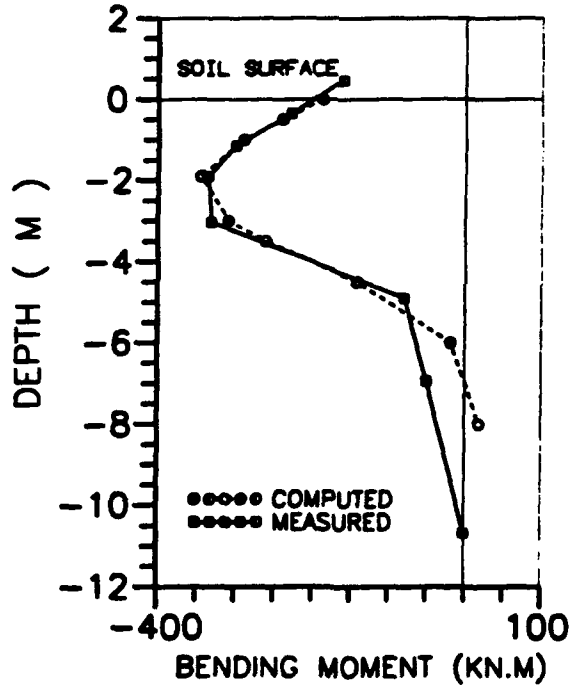

Fig. 7.8. The computed versus measured moment distribution of the pile at peak pile deflection.

then decrease to zero at a depth around 12.5 diameters. The moments along the pile have the same signs at any instant of time, suggesting that the inertial interaction caused by the pile head mass dominates response, and the pile is vibrating in its first mode. The peak moment predicted by the simplified 3-D finite element analysis is 344 kNm compared with a measured peak value of 325 kNm an error of only 6%.

It is interesting to show the degradation in shear modulus with shear strain around the pile during shaking. Distributions of moduli at specific depths and a specific time during the earthquake are shown in Fig. 7.9. The figures show that significant modulus degradation occurs near the pile and is most pronounced near the pile head.

Computational Time

Using a PC-486 (33 MHz) computer, the average CPU time needed to complete one integration step is 7 sec for the finite element grid shown in Fig. 7.3, and 3 hours of CPU time are required for the full input acceleration record of 1550 steps. The computational time would be shorter for a linear elastic analysis.

Pile Impedances During Strong Shaking

Dynamic impedances as functions of time were computed corresponding to the strain dependent shear moduli from the finite element analysis. Harmonic loads with an amplitude of unity were applied at the pile head, and the resulting equations were solved to obtain the complex valued pile impedances. The pile impedances were evaluated at the ground surface. This is the first time that the time histories of pile impedances during an earthquake have been determined.

single pile at 17.11 sec

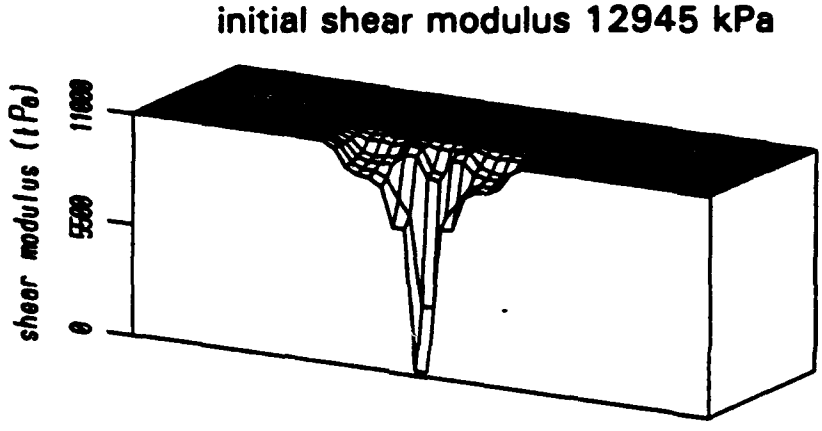

(a) at depth 0.25 m

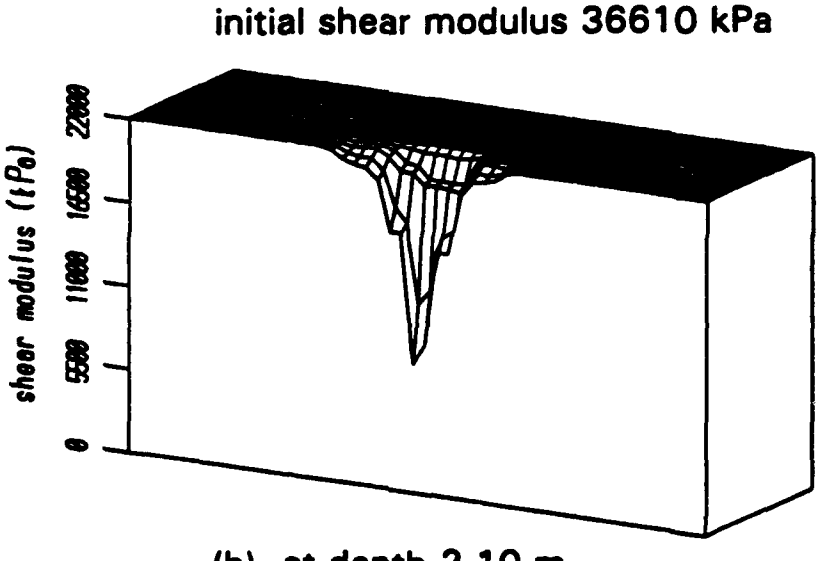

(b) at depth 2.10 m

Fig. 7.9. 3-D plots of the distribution of effective shear moduli with depth around a pile during dynamic excitation.

The dynamic stiffness of the pile decreases dramatically as the level of shaking increases (Fig. 7.10). The dynamic stiffnesses experience their lowest values between about 10 and 14 seconds, when the maximum accelerations occurs at the pile head. It can be seen that the lateral stiffness component k_{vv} decreased more than the rotational stiffness $k_{\theta\theta}$ or the coupled lateral-rotational stiffness $k_{v\theta}$. On the other hand the equivalent damping coefficients increased as the level of shaking increased because the hysteretic damping of the soil increased with increased strains.

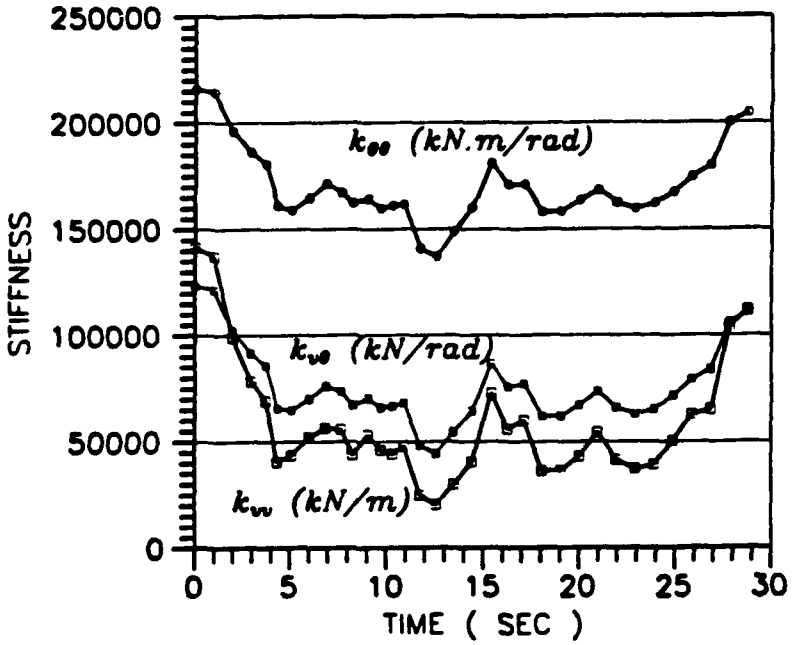

Fig. 7.10. Impedances k_{vv}, $k_{v\theta}$ and $k_{\theta\theta}$ of the single pile.

At its lowest level, k_{vv} decreased to 22,000 kN/m, only 15.2 % of its initial stiffness of 145,000 kN/m. $k_{v\theta}$ decreased to 45,000 kN/rad or 36% of its initial stiffness of 125,000 kN/rad.

$k_{\theta\theta}$ showed the least effect of shear strain. It decreased to 138,000 kN.m/rad or 63.6% of its initial stiffness of 217,000 kN.m/rad. The stiffnesses rebounded when the level of shaking decreased with time. Representative values of the pile stiffnesses k_{vv}, $k_{v\theta}$ and $k_{\theta\theta}$ that might be used in structural analyses may be taken as 40,000 kN/m, 65,000 kN/rad and 160,000 kN.m/rad, respectively. These stiffnesses are 32%, 52% and 73.7% of the original stiffnesses.

The effect of frequency on both stiffness and damping is explored for a range of frequencies from 1.91 Hz to 10 Hz at different times during the dynamic shaking of the pile. The stiffness response is shown in Fig. 7.11. Clearly within this range of frequencies which is typical of the frequencies of peak response in many near and medium field earthquake motions, there is no frequency effect on stiffness.

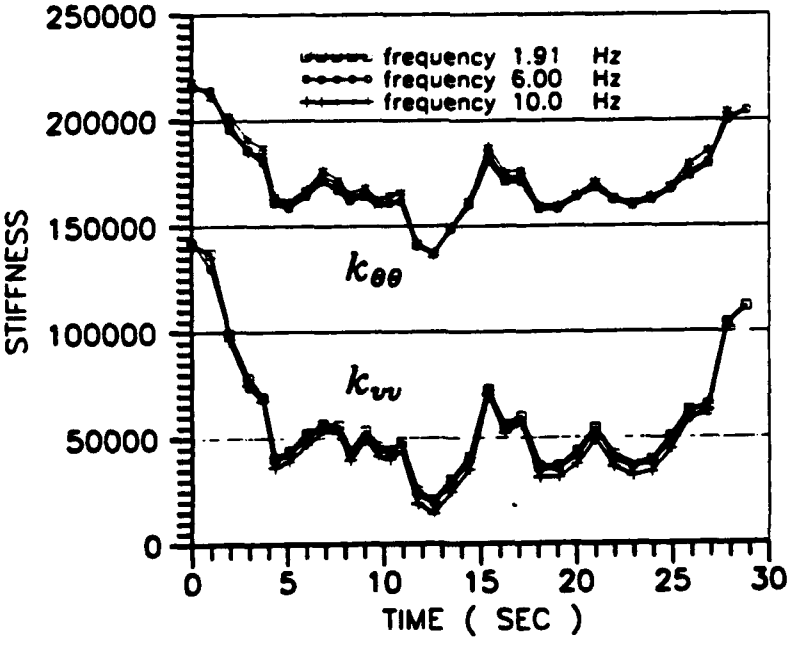

Fig. 7.11. Variation of pile head stiffnesses with frequency.

The damping response is shown in Fig. 7.12. Clearly, even within this relatively small frequency range there is a significant variation in the damping of the pile. This indicates that it is very difficult to select the proper equivalent dashpot to reflect the damping of a pile foundation in a structural analysis.

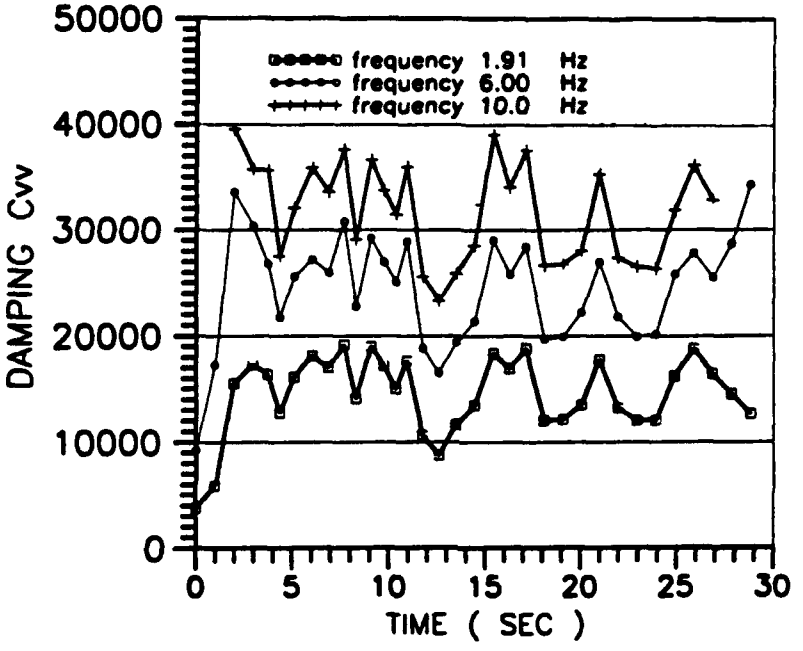

Fig. 7.12. The effect of frequency on pile damping.

The centrifuge test provides an opportunity to evaluate the effects of inertial interaction on the stiffness of a pile foundation. Many procedures in practice for evaluating pile stiffnesses are based on computing the inertial and kinematic components of soil structure interaction separately (Gazetas, 1991a, 1991b). This is acceptable for elastic response because the additional foundation excitation caused by the inertia of the structural mass does not affect the stiffness of the foundation. However, when there is nonlinear response of the foundation, the inertial

interaction of the structure with the foundation can cause major changes in foundation stiffness and in the period of peak response.

This is clearly shown by analysis of the single pile in the centrifuge test with and without the structural mass. The results of the analysis are shown in Fig. 7.13 which shows the significant degradation in pile stiffness due to inertial mass at the pile head for both translational and rotational stiffnesses, k_{vv} and $k_{\theta\theta}$, respectively. Clearly, for strong earthquake shaking the effects of inertial mass cannot be ignored and relying on kinematic stiffness only may lead to a serious overestimation of pile stiffness.

So far, validation of the simplified method of analysis has been done by comparing solutions with published elastic solutions using full 3-D formulations or by data from centrifuge tests. In conclusion, a forced vibration test on a full size pile in the field will now be analyzed.

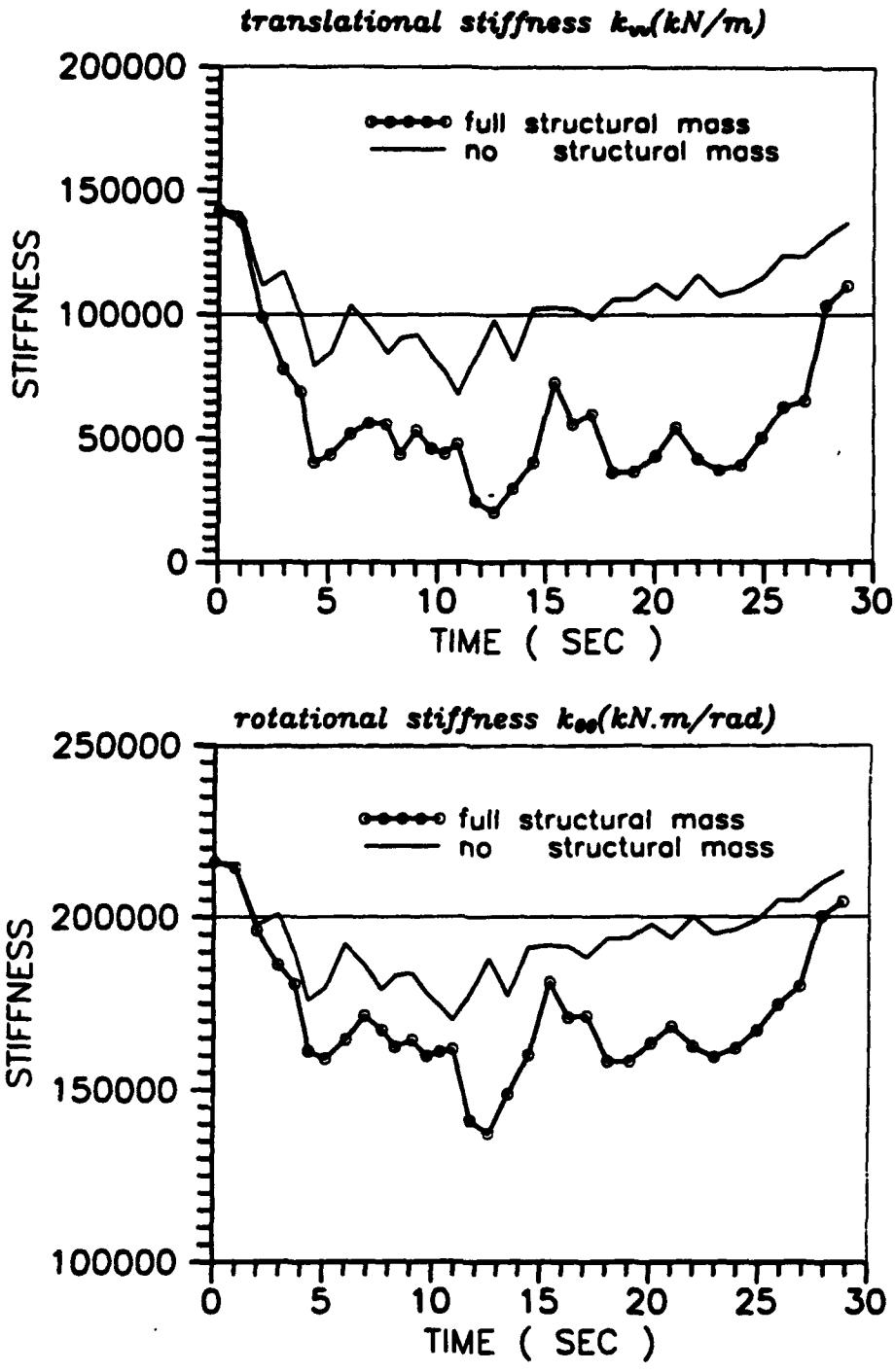

Fig. 7.13. The effect of inertial interaction on pile head stiffnesses.

CHAPTER 8

ANALYSIS OF FULL-SCALE VIBRATION TEST ON A FRANKI PILE

Test Set-Up

A full scale vibration test on a single Franki type pile was performed by Sy and Siu (1992) at the University of British Columbia Pile Research Facility located in the Fraser river delta just south of Vancouver, B.C.. The soil profile at the testing site consists of 4 m of sand and gravel fill overlying a 1 m thick silt layer over fine grained sand to a depth of 40 m. A seismic cone penetration test (SCPT 88-6) was conducted 0.9 m from the test pile. In addition, SPT tests were conducted in a mud-rotary drill hole (DH88-2) 2.4 m from the test pile. The measured in-situ shear wave velocity data are presented in Fig. 8.1, together with the cone penetration test (CPT) data and the Standard Penetration Test (SPT) data.

The layout of the pile test is shown in Fig. 8.2. The pile has an expanded spherical base with a nominal diameter of 0.93 m. For 6.4 m above the expanded base, the pile has a nominal diameter of 510 mm. The remaining length has a square cross-section with a side width of 510 mm. A structural mass consisting of 1.6 m cube of reinforced concrete was formed on top of the pile with a clearance of 150 mm above the ground surface.

Accelerometers were mounted on the shake mass and the pile cap to measure the dynamic input force and the pile cap responses as shown in Fig. 8.2. The vertical and coupled horizontal and rocking modes of vibration were obtained by rotating the shaker so that the dynamic forces were applied in the vertical and horizontal directions. The natural frequency of the cap-pile-soil system in each vibration mode was estimated by applying random bandwidth excitation. Then a

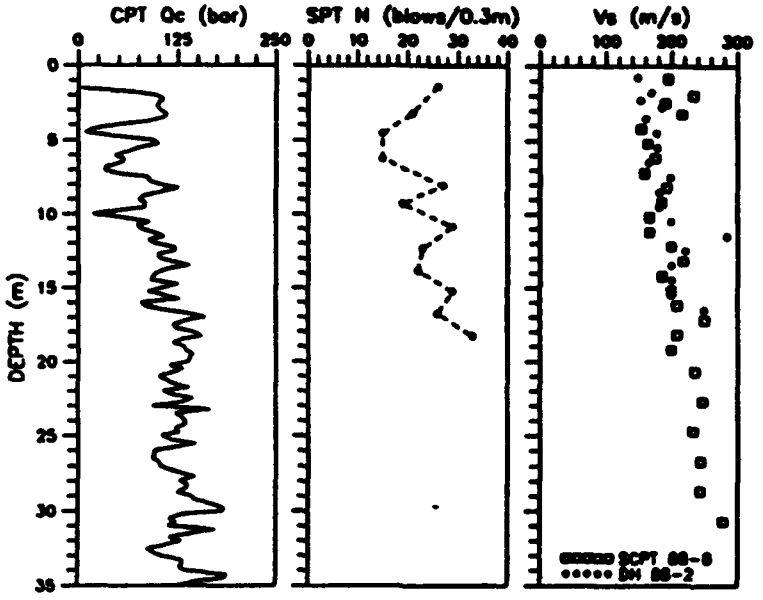

Fig. 8.1. The in-situ measured geotechnical data.

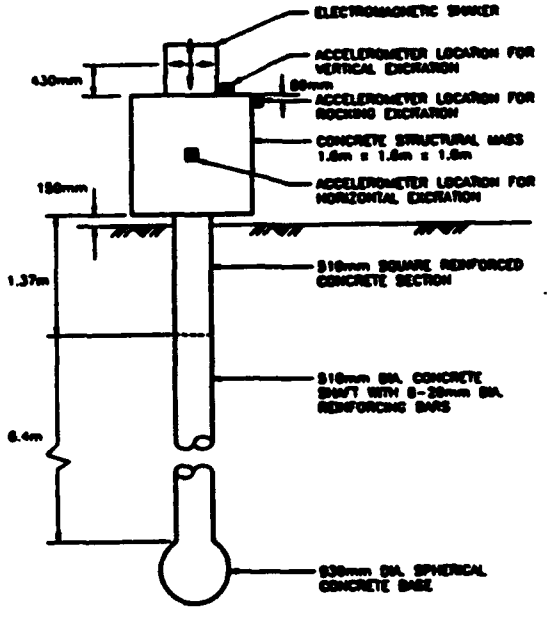

Fig. 8.2. The layout of the full-scale vibration test on a single pile.

detailed sinusoidal frequency sweep was carried out around the natural frequency indicated from the random bandwidth test.

The resonant frequencies from the sinusoidal sweep testing are evident in Fig. 8.3. The damping ratios are calculated from the measured frequency response curves shown in Fig. 8.3 using the half power point or bandwidth method (Clough and Penzien, 1975).

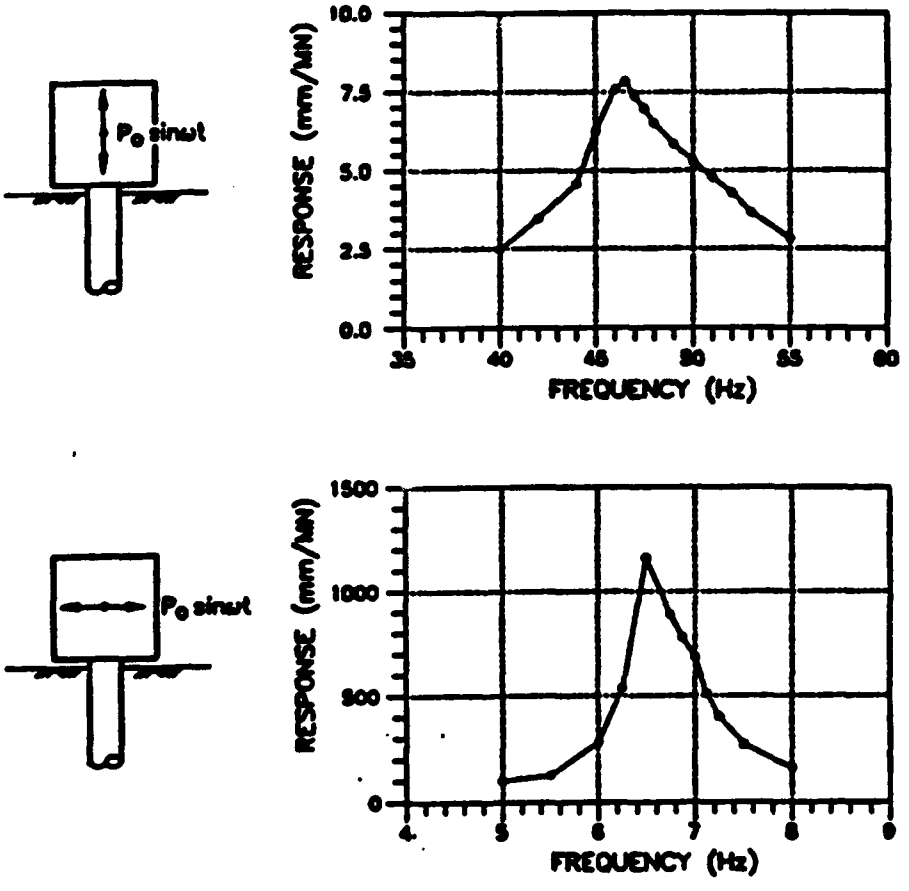

Fig. 8.3. The measured dynamic responses of the pile cap under sinusoidal input (after Sy and Siu, 1992).

Analysis of Tests

The structural properties of the pile cap and the test pile used in the analysis are presented in Table 8.1. The shear wave velocity V_s, unit weight γ, and damping ratio D_s used in the analysis are shown in Fig. 8.4. Following Sy and Siu (1992), an upper bound of the measured V_s values was used to account for the effect of soil densification caused by pile installation except for the top 1.2 m depth. V_s values in the upper 1.2 m were reduced, since the original soil around the extended pile shaft section was replaced by the loose backfill. A Poisson's ratio of 0.3 is assumed for all soil layers.

Table 8.1. Structural properties of pile cap and test pile (after Sy and Siu, 1992).

PARAMETER	UNIT	VALUE
PILE CAPE AND SHAKER		
Mass	Mg	10.118
Mass moment of inertia	Mg m^2	4.317
Height to centre of gravity	m	0.8
TEST PILE		
Top 1.37m: axial rigidity (EA)	MN	6350
Top 1.37m: flexural rigidity (EI)	MN m^2	141
1.37-7.77m: axial rigidity (EA)	MN	5150
1.37-7.77m: flexural rigidity (EI)	MN m^2	92
Base: axial rigidity (EA)	MN	14,720
Base: flexural rigidity (EA)	MN m^2	800
Material damping ratio		0.01
Poisson's ratio		0.25

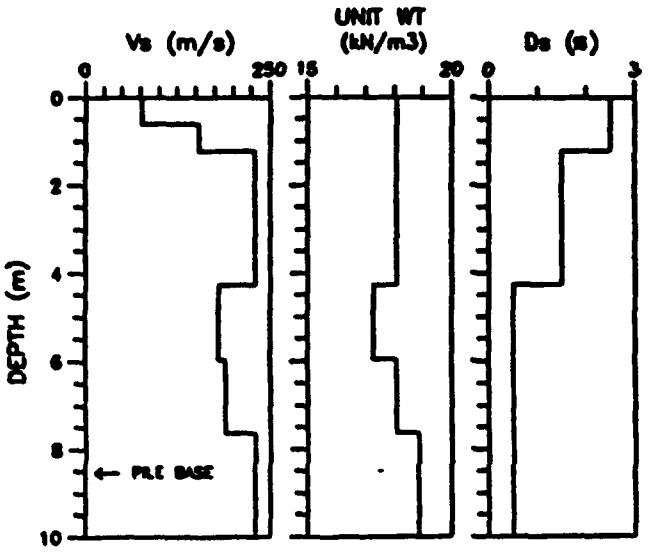

Fig. 8.4. The soil parameters used in analysis (Sy and Siu, 1992).

Figure 8.5 shows the 3-D finite element model used in present analysis. Due to symmetry, only half of the full mesh is needed. The finite element model consists of 1225 nodes and 889 elements. There is one beam element above the ground surface to represent the pile segment above the ground. The expanded base is modelled by a solid element rather than a beam element in the finite element analysis.

Since the pile behaves elastically under the very low excitation forces used in the test (F_{max} = 165 N), it is possible to use an uncoupled analysis and treat the pile foundation and the pile structure above the ground separately. First the pile impedances are determined as a function of frequency. Then the response of the mass on the pile head is computed incorporating the proper stiffness and damping components of the impedances depending on the frequency of the exciting force.

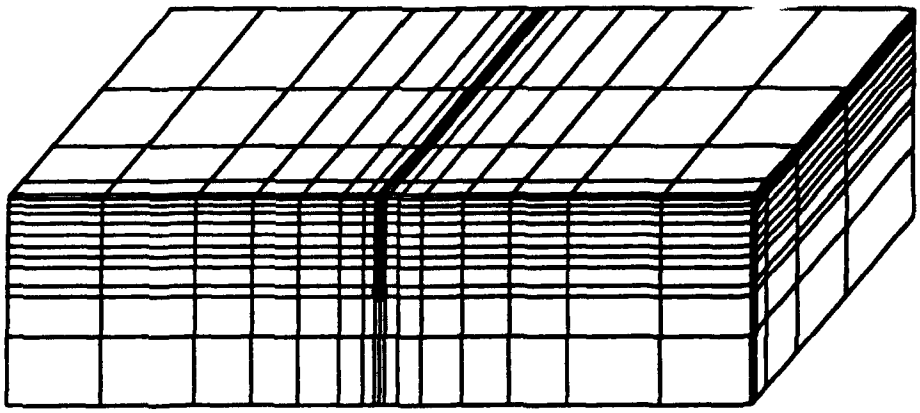

Fig. 8.5. Finite element model used in analysis.

The pile head impedances (stiffness and damping) of the pile foundation were computed using the proposed simplified 3-D finite element method. Harmonic force or moment with unit amplitude was applied at the pile head, and the resulting complex valued displacement at the pile head was determined. Impedances were then evaluated.

The horizontal and rocking responses of the pile head mass were obtained by using the two-degree of freedom system shown in Fig. 8.6(b). The coupled translation-rotation equation of motion in Eq. 8.1 describes the motion of the system.

$$-\omega^2\begin{bmatrix} m & m\cdot h_{cg} \\ m\cdot h_{cg} & I_{cg} \end{bmatrix}\begin{Bmatrix} v_p \\ \theta_p \end{Bmatrix}+\begin{bmatrix} k_{vv}+iC_{vv} & k_{v\theta}+iC_{v\theta} \\ k_{v\theta}+iC_{v\theta} & k_{\theta\theta}+iC_{\theta\theta} \end{bmatrix}\begin{Bmatrix} v_p \\ \theta_p \end{Bmatrix}=\begin{Bmatrix} P_0 \\ M_0 \end{Bmatrix} \qquad (8.1)$$

where m is the mass of the pile cap and shaker; h_{cg} is the height of the centre of gravity to the pile head; I_{cg} is the mass moment of inertia at the centre of gravity; k_{ij} and C_{ij} are the stiffnesses and

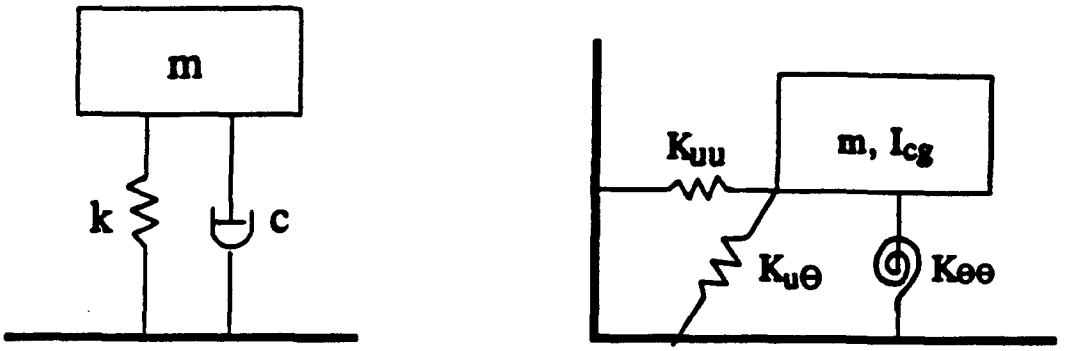

Fig. 8.6. Uncoupled systems for modelling the vertical motions (a), and the translational and rotational motions (b).

damping at the pile head; v_p and θ_p are the translation and rotation at the pile head; and P_0 and M_0 are amplitudes of the harmonic external force and moment, respectively, applied at the pile head.

Harmonic load amplitudes of 165 N in the horizontal direction with a coupled moment of 335 N.m were applied at the pile head to simulate conditions created by the test.

The horizontal displacement amplitude at the centre of gravity, v_{cg} is given by

$$v_{cg} = v_p + \theta \cdot h_{cg} \tag{8.2}$$

The analyses were carried out at different frequencies ω. The computed horizontal displacement amplitude versus frequency ω is shown in Fig. 8.7. A very clear and pronounced peak response is observed at a frequency of 6.67 Hz compared to the measured frequency of 6.5 Hz. The computed and measured fundamental frequencies and damping ratios for the translation and vertical modes of response are given in Table 8.2. The agreement between them is very good.

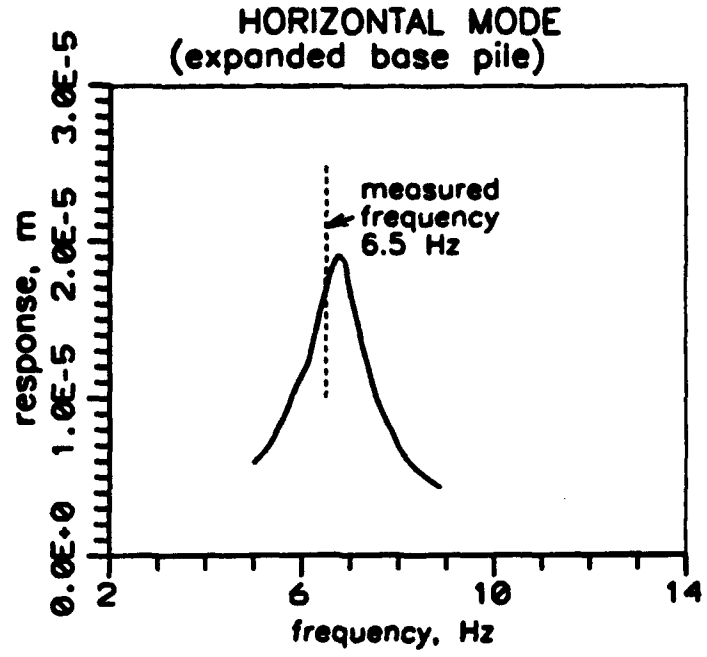

Fig. 8.7. Amplitudes of horizontal displacement at the centre of gravity of the pile cap versus the excitation frequency (first mode).

Table 8.2. Computed and measured resonant frequencies and damping ratios.

Mode of Excitation	Computed Resonant Frequency (Hz)	Measured Resonant Frequency (Hz)	Computed Damping Ratio	Calculated Damping Ratio
Vertical	44.0	46.5	0.04	0.05
Translational	6.67	6.50	0.06	0.04

CHAPTER 9

CONCLUSIONS

A simplified 3-D model of the response of a soil continuum to horizontal earthquake shaking has been developed which can simulate the important aspects of the seismic response with very good accuracy.

The model has been formulated in terms of finite elements and adapted for the dynamic analysis of piles by the incorporation of beam elements. Solutions can be obtained for both elastic and nonlinear soil response. Nonlinear response is modelled by maintaining compatibility between shear strains and effective moduli and damping throughout the dynamic analysis.

The modified 3-D model and its extension to dynamic analysis of piles was the original conception of Guoxi Wu. (1993).

The model has been validated for elastic response using existing exact elastic solutions. The soil continuum model alone has been validated using Wood's (1973) exact solution for dynamic pressures against rigid walls. The pile-soil model has been validated by comparing pile impedances for single piles computed by the model with those computed by Kaynia and Kausel (1982) using full 3-D continuum equations. Agreement between model solutions and the more exact solution is very good.

In the nonlinear mode, the model has been validated for single pile response using data from strong shaking tests on single pile foundations conducted on the centrifuge at the California Institute of Technology (Gohl, 1991). The important aspects of acceleration and moment time histories were simulated well by the model and the distribution of peak moments along the pile were within 6% of the measured moments.

The model simulated successfully the response of a full scale Franki type pile to forced vibration. The test was conducted at the University of British Columbia Pile Research Facility by Sy and Siu (1992).

The computational time for conducting analyses has been greatly reduced. Thus, the main objective of the Phase II studies has been achieved.

It now remains to extend the model to pile groups and to dynamic effective stress analysis. The latter feature will allow consideration of the effects of high porewater pressures on response.

REFERENCES

Finn, W.D. Liam, M. Yogendrakumar, N. Yoshida and H. Yoshida. (1986). "TARA-3: A Program for Nonlinear Static and Dynamic Effective Stress Analysis," Soil Dynamics Group, University of British Columbia, Vancouver, B.C., Canada.

Finn, W.D. Liam and W.B. Gohl. (1987). "Centrifuge Model Studies of Piles Under Simulated Earthquake Loading," from Dynamic Response of Pile Foundations - Experiment, Analysis and Observation, ASE Convention, Atlantic City, New Jersey, Geotechnical Special Publication No. 11, pp. 21-38.

Finn, W.D. Liam and M. Yogendrakumar. (1989). "TARA-3FL - Program for Analysis of Liquefaction Induced Flow Deformations," Department of Civil Engineering, University of British Columbia, Vancouver, B.C., Canada.

Finn, W.D. Liam, R.H. Ledbetter, R.L. Fleming Jr., A.E. Templeton, T.W. Forrest and S.T. Stacy. (1991). "Dam on Liquefiable Foundation: Safety Assessment and Remediation," Proceedings, 17th International Congress on Large Dams, Vienna, pp. 531-553, June .

Finn, W.D. Liam, Guoxi Wu and R.H. Ledbetter. (1994). "Problems in Seismic Soil Structure Interaction," Proc., 8th Int. Conference on Computer Methods and Advances in Geomechanics, Morgantown, West Virginia, USA, May, Balkema, Rotterdam, Vol. I, pp. 139-151.

Finn, W.D. Liam, Guoxi Wu and R.H. Ledbetter. (1994b). "Recent Developments in the Static and Dynamic Analysis of Pile Groups," Proc., Symposium on Deep Foundations, Vancouver Geotechnical Society, May.

Finn, W.D. Liam and Guoxi Wu, (1994). "Recent Developments in the Dynamic Analysis of Piles," Proc., Japanese Earthquake Symposium, Tokyo, 1994.

Gazetas, G., K. Fan, and A. Kaynia, (1993). "Dynamic Response of Pile Groups with Different Configurations," Soil Dynamics and Earthquake Engineering, No. 12, pp. 239-257.

Gazetas, G. and M. Makris, (1991a). "Dynamic Pile-Soil-Pile Interaction. Part I: Analysis of Axial Vibration," Earthquake Engineering Struct. Dyn., Vol. 20, No. 2, pp. 115-132.

Gazetas, G., M. Makris, and E. Kausel, (1991b). "Dynamic Interaction Factors for Floating Pile Groups," J. Geotech. Eng., ASCE, Vol. 117, No. 10, pp. 1531-1548.

Gohl, W.B. (1991). "Response of Pile Foundations to Simulated Earthquake Loading: Experimental and Analytical Results," Ph.D. Thesis, Dept. of Civil Engineering, University of British Columbia, Vancouver, B.C., Canada.

Hardin, B.O. and W.L. Black, (1968). "Vibration Modulus of Normally Consolidated Clay," ASCE, J. Soil Mechanics and Foundations Division, Vol. 94, pp. 353-369.

Idriss, I.M., H.B. Seed and N. Serff, (1974). "Seismic Response by Variable Damping Finite Elements," Journal of Geotechnical Engineering Division, ASCE, Vol. 100, No. 1, pp. 1-13.

Kaynia, A.M. and E. Kausel. (1982). "Dynamic Behaviour of Pile Groups," 2nd Int. Conf. on Num. Methods in Offshore Piling, Austin, TX, pp. 509-532.

Matsuo, H. and S. Ohara, (1960). "Lateral Earthquake Pressure and Stability of Quay Walls During Earthquakes," Proceedings, 2nd World Conference on Earthquake Engineering, Vol. 2.

Novak, M. (1991). "Piles Under Dynamic Loads," State of the Art Paper, 2nd Int. Conf. on Recent Advances in Geotech. Earthq. Eng. and Soil Dyn., University of Missouri-Rolla, Rolla, Missouri, Vol. III, pp. 250-273.

Schnabel, P.B., J. Lysmer and H.B. Seed (1972). "SHAKE: A Computer Program for Earthquake Response Analysis of Horizontally Layered Sites," Report EERC 71-12, University of California at Berkeley.

Seed, H.B. and I.M. Idriss, (1970). "Soil Moduli and Damping Factors for Dynamic Response Analyses," Report No. EERC 70-10, Earthquake Engineering Research Center, University of California, Berkeley, California.

Sy, A. and D. Siu, (1992). "Forced Vibration Testing of An Expanded Base Concrete Pile," Piles Under Dynamic Loads, ASCE Geotech. Special Publication No. 34, 170-186.

Veletsos, A.S. and A.H. Younan, (1994). "Dynamic Soil Pressures on Rigid Vertical Walls," Earthquake Engineering and Structural Dynamics, Vol. 23, No. 3, John Wiley & Sons, Ltd., pp. 275-301.

Wood, J.H. (1973). Earthquake-Induced Soil Pressures on Structures. Ph.D. Thesis, submitted to the California Institute of Technology, Pasadena, California.

Wu, G. (1993). Ph.D. Thesis (research continuing), Department. of Civil Engineering, University of British Columbia, Vancouver, B.C.